

TRANSITION PATH THEORY FOR LANGEVIN DYNAMICS ON MANIFOLD: OPTIMAL CONTROL AND DATA-DRIVEN SOLVER

YUAN GAO, TIEJUN LI, XIAOGUANG LI, AND JIAN-GUO LIU

ABSTRACT. We present a data-driven point of view for the rare events, which represent conformational transitions in biochemical reactions modeled by over-damped Langevin dynamics on manifolds in high dimensions. Given the point clouds sampled from an unknown reaction dynamics, we construct a discrete Markov process based on an approximated Voronoi tessellation which incorporates both the equilibrium and the manifold information. We reinterpret the transition state theory and transition path theory from the optimal control viewpoint. The controlled random walk on point clouds is utilized to simulate the transition path, which becomes an almost sure event instead of a rare event in the original reaction dynamics. Some numerical examples on sphere and torus are conducted to illustrate the data-driven solver for transition path theory on point clouds. The resulting dominated transition path highly coincides with the mean transition path obtained via the controlled Monte Carlo simulations.

1. INTRODUCTION

Complex molecular dynamics in chemical/biochemical reactions usually have cascades of timescales. For instance, the molecular vibrations occur in femtosecond time scale, while the conformational transitions occur in microsecond time scale. Assume the states $\{\mathbf{x}(t)\}$ of the original molecular dynamics are in a high dimensional space \mathbb{R}^p , and suppose the most important slow dynamics such as conformational transitions can be described by a reduced over-damped Langevin dynamics in terms of reaction coordinates \mathbf{y} on an intrinsic low-dimensional manifold $\mathcal{N} \subset \mathbb{R}^\ell$, where $\ell \ll p$ [CL06]. Then the slow dynamics on \mathcal{N} is guided by a reduced free energy $U_{\mathcal{N}}(\mathbf{y})$, $\mathbf{y} \in \mathcal{N}$, whose local minimums indicate several metastable states (say a, b) of the dynamics. Those conformational transitions from one metastable state a to another metastable state b are rare (but significant) events compared with typical relaxation dynamics in each energy basin. Thus efficient simulation and computation of transition rates or reaction pathways for the conformational transitions are challenging and important problems, which has been one of the core subjects in applied mathematics in recent years; see recent review in [EVE10].

To make the discussion precise, we denote the over-damped Langevin dynamics of \mathbf{y} by

$$(1.1) \quad d\mathbf{y}_t = -\nabla_{\mathcal{N}} \cdot U_{\mathcal{N}}(\mathbf{y}_t) dt + \sqrt{2\varepsilon} \sum_{i=1}^d \tau_i^{\mathcal{N}}(\mathbf{y}_t) \otimes \tau_i^{\mathcal{N}}(\mathbf{y}_t) \circ dB_t,$$

where $\varepsilon > 0$ corresponds to the thermal energy in physics, the symbol \circ means the Stratonovich integral, B_t is ℓ -dimensional Brownian motion, d is the intrinsic dimension of the manifold \mathcal{N} and $\{\tau_i^{\mathcal{N}}; 1 \leq i \leq d\}$ are orthonormal basis of tangent plane $T_{\mathbf{y}_t}\mathcal{N}$. Here $\nabla_{\mathcal{N}} := \sum_{i=1}^d \tau_i^{\mathcal{N}} \nabla_{\tau_i^{\mathcal{N}}} = \sum_{i=1}^d \tau_i^{\mathcal{N}} \otimes \tau_i^{\mathcal{N}} \nabla$ is the surface gradient and $\nabla_{\tau_i^{\mathcal{N}}} = \tau_i^{\mathcal{N}} \cdot \nabla$ is the tangential derivative in the direction of $\tau_i^{\mathcal{N}}$. Given the manifold \mathcal{N} and potential $U_{\mathcal{N}}(\mathbf{y})$, when ε is small, the study of

2010 *Mathematics Subject Classification.* 60J22, 65C05, 60H30, 93E20.

Key words and phrases. Reaction rates, minimum energy path, committor function, controlled Markov process, realize rare events almost surely, nonlinear dimension reduction.

rare events by direct simulation of (1.1) is not feasible. This motivates the need of theoretical developments. In the limit $\varepsilon \rightarrow 0$, the optimal transition path problem can be well described through the large deviation theory [FW12]. This was formulated as the minimum action method (MAM) [ERVE04], and was extended to the manifold case in [LLZ16]. In the gradient case, the optimal transition path by MAM is actually the minimal energy path (MEP) connecting two metastable states, which was realized by the string method [ERVE02]. The string method was further extended to the finite ε case, i.e. the finite temperature string method for gradient systems [ERVE05]. In the general finite noise case, the transition path theory (TPT) was first proposed by E AND VANDEN-EIJNDEN in [EVE06] to obtain the transition paths and transition rates, etc., by the committor function q (see (3.1)). A mathematically rigorous interpretation of TPT was given in [LN15] (see precise statement in [LN15, Theorem 1.7]). The generalization of TPT to Markov jump process was given in [MSVE09].

We are concerning the rare event study from a data-driven point of view in this paper. In many cases, the manifold \mathcal{N} is not explicitly known and we assume only the point clouds $\{\mathbf{x}_i\}_{i=1:n}$ are available from some physical dynamics on an unknown d dimensional closed Riemannian submanifold $\mathcal{M} \subset \mathbb{R}^p$. By nonlinear dimension reduction algorithms such as diffusion map, one can learn the reaction coordinates $\mathbf{y} = \Phi(\mathbf{x}) : \mathcal{M} \hookrightarrow \mathbb{R}^\ell$ by using $\{\mathbf{x}_i\}_{i=1:n}$ in \mathbb{R}^p . Thus $\mathcal{N} = \Phi(\mathcal{M})$ is a submanifold of \mathbb{R}^ℓ and one can represent the high dimensional data $\{\mathbf{x}_i\} \subset \mathcal{M} \subset \mathbb{R}^p$ as $\mathbf{y}_i = \Phi(\mathbf{x}_i) \subset \mathcal{N} \subset \mathbb{R}^\ell$ in the low dimensional space. With the learned reaction coordinates \mathbf{y} , the main goal is to effectively simulate the conformational transitions on \mathcal{N} .

Our main contributions are in two folds: (i) the *optimal control reinterpretations of the committor function* in TPT; (ii) a *data-driven solver for finding transition paths on manifolds and compared with the controlled Monte Carlo simulations*. They are detailed as below.

Interpretation from optimal control viewpoint. The study of rare events from the optimal control viewpoint was pioneered in [HS12, HBS⁺13] and further investigated in [HSZ16, HRSZ17]. Our goal in this part is to rigorously reformulate the effective conditioned process - constructed from committor function q by [LN15] - as a stochastic optimal controlled process, in which the optimal feedback controls the original Markov process from one stable basin A to another stable basin B of the energy landscape $U_{\mathcal{N}}$ with minimum cost. Before doing this, we first reformulate the MEP finding problem from metastable states $a \in A$ to $b \in B$ as a deterministic optimal control problem by considering a controlled ODE with minimum cost (2.3) in the infinite time horizon. For the system described by a Markov process \mathbf{y} on manifold \mathcal{N} , e.g. (1.1), it will induce a measure on the path space $C([0, +\infty); \mathcal{N})$, which can be regarded as a prior measure P . Then we need to construct a new Markov process $\tilde{\mathbf{y}}$ (see controlled process in (3.15)), which induces a new measure \tilde{P} on the path space. The additional control drives the trajectory $\tilde{\mathbf{y}}$ from A to B almost surely, while the transitions for the original process are rare events. From the stochastic optimal control viewpoint, we need to find a control function $\mathbf{v}(\tilde{\mathbf{y}}_t)$ to realize the optimal change of measure from P to \tilde{P} such that the running cost (kinetic energy) and terminal cost (boundary cost hitting the basin) are minimized. In Section 3.2 and Theorem 3.2, we will prove the forward committor function q gives such an optimal control $\mathbf{v}^* = 2\varepsilon \frac{\nabla q}{q}$ that realizes the optimal change of measure on path space and thus realizes the transitions almost surely. These results also provide the basis for computing the transition path through the Monte Carlo simulations for the controlled random walk and the local average mean path algorithm in the second part.

Data-driven solver for transition path on manifolds. Without the exact manifold information, we need to first construct an approximated Markov process on manifold \mathcal{N} based on the Voronoi tessellation on point clouds, then perform the continued simulations. Our goal in this part is to study the optimal control problem above in its discrete analogies and construct a data-driven solver which efficiently finds the transition path on a manifold. Given the point clouds $\{\mathbf{y}_i\}_{i=1:n}$, we construct a discrete Markov process on $\{\mathbf{y}_i\} \in \mathcal{N}$ based on an approximated Voronoi tessellation for \mathcal{N} , which incorporates both the equilibrium and manifold information. More importantly, the assigned transition probability between the nearest neighbor points (adjacent points identified by Voronoi tessellation) enables us to efficiently compute the discrete committor function q_i and related quantities. In Section 4.2, based on the constructed discrete Markov process, we derive the discrete analogy of the optimal controlled Markov process on point clouds with the associated controlled generator. This enables an efficient controlled Monte Carlo simulations for the new almost sure event instead of the rare event in the original process. Then we design a local average mean path algorithm based on the collected samples, which highly coincides with the dominated transition path in TPT. The numerical construction of the approximated Markov process, TPT analysis and the local average mean path algorithm based on the controlled process sampling for the rare transitions on sphere and torus with Mueller potential are given in Section 5.

The rest of this paper is organized as follows. In Sections 2-3, we will make the connections between the optimal control theory and the transition state theory and the transition path theory, respectively. In Section 4, we present the constructions of the discrete original/controlled Markov process on point clouds. In Section 5, we present the detailed algorithms and the corresponding numerical examples to show the validity of the proposed algorithms.

2. OPTIMAL CONTROL VIEWPOINT FOR THE TRANSITION STATE THEORY

In this section, we will first consider the typical energy landscape $U_{\mathcal{N}}$ which indicates two metastable states and guides the Langevin dynamics on \mathcal{N} (see Section 2.1). Then we reformulate and solve the minimal energy path in the transition state theory from the deterministic optimal control viewpoint in Section 2.2. In Section 2.3, we briefly review the basic concepts for a stochastic optimal control problem in the infinite time horizon.

2.1. Energy landscape in the transition state theory. A chemical reaction from reactants $a \in \mathcal{N}$ through a transition state $c \in \mathcal{N}$ to products $b \in \mathcal{N}$ can be described by the reaction coordinate \mathbf{y} and a path on the reaction coordinate $\mathbf{y}(t) \in \mathcal{N}$ with a pseudo-time $t \in [0, T]$ and $\mathbf{y}(0) = a$, $\mathbf{y}(T) = b$. This chemical reaction can be characterized by an underlying potential $U(\mathbf{y})$ in terms of the reaction coordinate $\mathbf{y} \in \mathcal{N}$, which has a few deep wells separated by high barriers. Assume a and b are two local minimums with attractor basins $A, B \subset \mathcal{N}$ such that $\max(U_{\mathcal{N}}(a), U_{\mathcal{N}}(b)) < \min U(\partial A \cup \partial B)$. The associated mountain path is a path with minimal energy barrier given by

$$(2.1) \quad \mathbf{y}^* = \operatorname{argmin}_{\mathbf{y}} \max_{t \in [0, T]} U_{\mathcal{N}}(\mathbf{y}(t)),$$

and the transition state is given by

$$(2.2) \quad c = \operatorname{argmax}_{\mathbf{y}^*(t), t \in [0, 1]} U_{\mathcal{N}}(\mathbf{y}^*(t)).$$

Assume $U_{\mathcal{N}}$ is a Morse function and the Morse index at c is 1, i.e., there is only one negative eigenvalue (denoted as λ_c) for the Hessian matrix of $U_{\mathcal{N}}$ in the neighborhood of c . The energy

barrier to achieve the chemical reaction from a to b is $U_{\mathcal{N}}(c) - U_{\mathcal{N}}(a)$. The existence of the mountain path is guaranteed by the mountain pass theorem [Eva10], which is the foundation of calculating the transition state c , and we know c is a saddle point of $U_{\mathcal{N}}$.

By [FW12], the minimal energy path is given by the least action

$$(2.3) \quad \inf_{T>0} \inf_{\mathbf{y} \in C[0,T]; \mathbf{y}(0)=a, \mathbf{y}(T)=b} \int_0^T \frac{1}{2} |\dot{\mathbf{y}} + \nabla U_{\mathcal{N}}(\mathbf{y})|^2 dt.$$

For notation simplicity, from now on we use U as the shorthand notation of $U_{\mathcal{N}}$, ∇ as shorthand notation of $\nabla_{\mathcal{N}}$ and $\nabla \cdot$ as shorthand notation of the surface divergence defined as $\nabla_{\mathcal{N}} \cdot \xi = \sum_{i=1}^d \tau_i^{\mathcal{N}} \cdot \nabla_{\tau_i^{\mathcal{N}}} \xi$. In the case that U is a double-well potential with a, b being two local minimums, the minimal energy path (MEP) is given by the combination of the solutions $\mathbf{y}(t), t \geq 0$ to [FW12]

$$(2.4) \quad \begin{aligned} \dot{\mathbf{y}} &= \nabla U(\mathbf{y}), & \mathbf{y}(-\infty) &= a, \mathbf{y}(+\infty) = c, \\ \dot{\mathbf{y}} &= -\nabla U(\mathbf{y}), & \mathbf{y}(-\infty) &= c, \mathbf{y}(+\infty) = b. \end{aligned}$$

2.2. Minimal energy path as a deterministic optimal control problem. One can recast the least action problem (2.3) as a deterministic optimal control problem, which determines the optimal trajectory \mathbf{y} , the feedback control \mathbf{v} , and the optimal terminal time T . Since the original dynamics is translation invariant w.r.t. time (stationary), we introduce the control variable $\mathbf{v} = \mathbf{v}(\mathbf{y}(t))$. The least action problem in (2.3) is equivalent to the following optimal control problem with running cost $L = \frac{1}{2} |\mathbf{v}|^2$

$$(2.5) \quad \begin{aligned} \gamma &= \inf_{T, \mathbf{v}} \int_0^T \frac{1}{2} |\mathbf{v}(\mathbf{y}(t))|^2 dt \\ \text{s. t. } \dot{\mathbf{y}} &= \mathbf{v}(\mathbf{y}) - \nabla U(\mathbf{y}), \quad t \in (0, T), \quad \mathbf{y}(0) = a, \mathbf{y}(T) = b. \end{aligned}$$

Here $\mathbf{v}(\mathbf{y})$ belongs to the C^1 tangent vector field on \mathcal{N} . Define the augmented Lagrangian function as

$$(2.6) \quad \mathcal{L}(\mathbf{y}, \dot{\mathbf{y}}, \mathbf{v}, \lambda) := \frac{1}{2} |\mathbf{v}|^2 - \lambda(t) \cdot (\dot{\mathbf{y}} - \mathbf{v}(\mathbf{y}) + \nabla U(\mathbf{y})),$$

where $\lambda(t)$ is the Lagrange multiplier. Then the corresponding Hamiltonian is

$$(2.7) \quad \mathcal{H}(\mathbf{y}, \mathbf{v}, \lambda) := \mathcal{L} - \dot{\mathbf{y}} \cdot \frac{\partial \mathcal{L}}{\partial \dot{\mathbf{y}}} = \frac{1}{2} |\mathbf{v}|^2 + \lambda \cdot (\mathbf{v}(\mathbf{y}) - \nabla U(\mathbf{y})).$$

Then calculating the first variation of $\int_0^T \mathcal{L} dt$ with respect to perturbations $\tilde{\mathbf{y}}, \tilde{\mathbf{v}}, \tilde{\lambda}, \tilde{T}$ gives the Euler-Lagrange equation to (2.5)

$$(2.8) \quad \frac{\partial \mathcal{L}}{\partial \mathbf{y}} - \frac{d}{dt} \left(\frac{\partial \mathcal{L}}{\partial \dot{\mathbf{y}}} \right) = 0, \quad \frac{\partial \mathcal{L}}{\partial \mathbf{v}} = 0, \quad \frac{\partial \mathcal{L}}{\partial \lambda} = 0, \quad \mathcal{H}(T_*) = 0,$$

which can be further simplified as

$$(2.9) \quad \begin{aligned} \dot{\mathbf{v}} &= \nabla^2 U(\mathbf{y}) \mathbf{v}, \\ \dot{\mathbf{y}} &= \mathbf{v} - \nabla U(\mathbf{y}), \\ \mathbf{y}(0) &= a, \quad \mathbf{y}(T) = b, \\ -\frac{|\mathbf{v}|^2}{2} + \nabla U(\mathbf{y}) \cdot \mathbf{v} \Big|_{t=T_*} &= 0. \end{aligned}$$

By the Pontryagin maximum principle, the Euler-Lagrange equation can be expressed in terms of the corresponding Hamiltonian \mathcal{H}

$$(2.10) \quad \frac{d}{dt}\mathbf{y} = \frac{\partial \mathcal{H}}{\partial \lambda}, \quad \frac{d}{dt}\lambda = -\frac{\partial \mathcal{H}}{\partial \mathbf{y}}, \quad \frac{\partial \mathcal{H}}{\partial \mathbf{v}} = 0, \quad \mathcal{H}(T_*) = 0.$$

It is easy to see the Hamiltonian is a constant, so the last equation in (2.9) holds for all $0 \leq t \leq T$, i.e.

$$(2.11) \quad |\mathbf{v} - \nabla U(\mathbf{y})|^2 = |\nabla U(\mathbf{y})|^2.$$

Recall the transition state (saddle point) c in (2.2) is obtained by the mountain pass theorem. The minimum value of $\int_0^T |\mathbf{v}|^2 dt = 2(U(c) - U(a))$ is achieved when the optimal control \mathbf{v} in (2.11) takes $\mathbf{v} = 2\nabla U(\mathbf{y})$ before the transition state c while it takes $\mathbf{v} = 0$ after passing the transition state c . Indeed, one can verify the optimality as follows. For any path from A to B , it must pass a point \mathbf{y}_s such that $U(\mathbf{y}_s) \geq U(c)$ due to the mountain pass theorem. Denote $T_{\mathbf{y}_s}$ the time passing \mathbf{y}_s , then from (2.5), we have

$$(2.12) \quad \begin{aligned} \int_0^T \frac{1}{2} |\mathbf{v}|^2 dt &\geq \int_0^{T_{\mathbf{y}_s}} \frac{1}{2} |\mathbf{v}|^2 dt = \frac{1}{2} \int_0^{T_{\mathbf{y}_s}} |\dot{\mathbf{y}} - \nabla U(\mathbf{y})|^2 + 2 \int_0^{T_{\mathbf{y}_s}} \dot{\mathbf{y}} \cdot \nabla U(\mathbf{y}) dt \\ &\geq 2 \int_0^{T_{\mathbf{y}_s}} \frac{d}{dt} U(\mathbf{y}) dt = 2(U(\mathbf{y}_s) - U(a)) \geq 2(U(c) - U(a)). \end{aligned}$$

This inequality shows that the minimal energy barrier (a.k.a. value function) is $\gamma = 2(U(c) - U(a))$ and the minimal energy path must pass through c . This is consistent with the MEP given in (2.4). Notice the transition state c is the critical point of U , so the

$$(2.13) \quad \dot{\mathbf{y}}|_{\mathbf{y}=c} = (\mathbf{v} - \nabla U(\mathbf{y}))|_{\mathbf{y}=c} = 0.$$

Hence c is the critical point of the optimal path, at which the trajectory stays for most of the time. We remark the stochastic control problem in Theorem 3.2 later is the stochastic version of the control problem (2.5); see [FS06] and Remark 3.3 after Theorem 3.2.

2.3. General stochastic optimal control problems with terminal cost. In general, one can consider a stochastic optimal control problem with some running cost function $L(t, \mathbf{y}_t)$ and terminal cost function $g(T, \mathbf{y}_T)$, where we have used the convention $\mathbf{y}_t := \mathbf{y}(t)$ in stochastic analysis. Especially, we are interested in the optimal control for a stationary (w.r.t. time) Markov process and the terminal time being the stopping time when the SDE solution hitting some closed set B , i.e. $\tau := \inf\{t \geq 0; \mathbf{y}_t \in B\}$. In this case, the terminal cost function g is also called boundary cost function, to be specific in Theorem 3.2.

Given initial probability measure μ_0 on \mathcal{N} concentrating on the local minimums a of the potential U , consider the stochastic optimal control problem in the infinite time horizon with running cost function $\frac{1}{2}|\mathbf{v}(\mathbf{y}_t)|^2$ and boundary cost function $g(\mathbf{y}_\tau)$

$$(2.14) \quad \begin{aligned} \gamma &= \inf_{\mathbf{v}} \mathbb{E} \left\{ \int_0^\tau \frac{1}{2} |\mathbf{v}(\mathbf{y}_t)|^2 dt + \chi_{\tau < \infty} g(\mathbf{y}_\tau) \right\} \\ \text{s. t. } d\mathbf{y}_t &= (-\nabla U(\mathbf{y}_t) + \mathbf{v}(\mathbf{y}_t)) dt + \sqrt{2\varepsilon} d_{\mathcal{N}} B_t, \quad t \in (0, \tau), \quad \mathbf{y}_t|_{t=0} \sim \mu_0. \end{aligned}$$

Here $|\mathbf{v}|$ is the length of \mathbf{v} in \mathbb{R}^ℓ and $d_{\mathcal{N}} B_t$ is a shorthand notation for the Brownian motion on manifold \mathcal{N} in the sense of (1.1), which will be used in the following context. In Nelson's theory of stochastic mechanics, v can be regarded as an average velocity and the running cost function $L = \frac{1}{2}|\mathbf{v}|^2$ is the classical action integrand including only kinetic energy. The obtained optimal control $\mathbf{v}(\mathbf{y})$ is called stationary Markov control policy. Since the original Markov process is

on a closed manifold \mathcal{N} , we will always has the recurrence property provided the landscape is continuous. From now on, we focus on the case $\tau < \infty$, a.s..

With the small parameter ε , recall the original Markov process Y_t on manifold \mathcal{N} without control has the corresponding generator $Qf = \varepsilon\Delta f - \nabla U \cdot \nabla f$. The control \mathbf{v} in the stochastic control problem (2.14) can be regarded as an additional driven force to the original Markov process. Suppose $\mathbf{y}_t \sim \mu_t$. Then μ_t satisfies the transport equation with diffusion

$$(2.15) \quad \partial_t \mu_t + \nabla \cdot ((-\nabla U + \mathbf{v})\mu_t) = \varepsilon \Delta \mu_t.$$

Thus (2.14) is recast to

$$(2.16) \quad \inf_{\mathbf{v}} \int_{\mathcal{N}} \int_0^\tau |\mathbf{v}|^2 d\mu_t dt$$

s. t. $\partial_t \mu_t + \nabla \cdot ((-\nabla U + \mathbf{v})\mu_t) = \varepsilon \Delta \mu_t, \quad t \in (0, \tau), \quad \mu_0 = \mu_0.$

3. OPTIMAL CONTROL VIEWPOINT FOR THE TRANSITION PATH THEORY FOR THE CONTINUOUS MARKOV PROCESS

In this section, the main goal is to give a stochastic optimal control interpretation for the transition path theory. We will first review the transition path theory in Section 3.1. Then in Section 3.2, we prove the committor function in the transition path theory leads to a stochastic optimal control with which the controlled Markov process realizes the transitions from A to B almost surely.

3.1. Review of the transition path theory. Now we review and explain some concepts in the transition path theory including the committor function, the effective transition path process, and the density/current of transition paths; see original work [EVE06] .

3.1.1. Committor function. We start from the original Markov process Y_t with generator $Qf = \varepsilon\Delta f - \nabla U \cdot \nabla f$. Recall A and B are the basins of attractors a, b . To study the conditioned process with the conditions on paths starting from A then ending in B , one should find an appropriate excessive function q and calculate the transition probabilities of the conditioned process by using Doob h -transformation via q .

Remark 3.1. As mentioned in Section 2.3, we know the SDE solution Y_t hits $\overline{A \cup B}$ at a finite time due to the recurrence of the process Y_t on the closed manifold \mathcal{N} . For an unbounded domain, the recurrence can be ensured by some specific condition, for instance,

$$\nabla_{\mathbf{n}} U \Big|_{|\mathbf{y}|=r} > \frac{c}{r}, \quad \text{for some } c > \frac{d}{2} + 1.$$

Here $|\mathbf{y}| = r$ is the geodesic ball on \mathcal{N} and $\mathbf{n} \in T_{\mathcal{N}}$ is the normal vector of the ball.

Define the stopping time $\tau_B := \inf\{t \geq 0; Y_t \in \bar{B}\}$ (resp. τ_A) of process Y_t when it hits B (resp. A). The probability for the paths hitting B before A is given by the forward committor function $q(\mathbf{y})$, a.k.a. harmonic potential, which is the solution of

$$(3.1) \quad Qq(\mathbf{y}) = 0, \quad \mathbf{y} \in (\overline{A \cup B})^c$$

with the Dirichlet boundary conditions $q(\mathbf{y}) = 0, \mathbf{y} \in \bar{A}$ while $q(\mathbf{y}) = 1, \mathbf{y} \in \bar{B}$.

As an important consequence, the density and the current of transition paths can be calculated using the committor function; see detailed revisit in Section 3.1.3.

3.1.2. *Generator for the conditioned process.* To describe the conditioned process with the conditions that paths starting from A then ending in B , [LN15] characterized the selection of the reactive paths coming from A and then hitting B by using the probability measure on the path space such that $\tau_A > \tau_B$.

The associated conditioned process, called transition path process, is denoted as Z_t . For $Z_0 = \mathbf{y}_0 \in (\overline{A \cup B})^c$, the generator of this conditioned process Z_t can be described using the Doob h -transformation. Precisely, using committor function q as the excessive function and by the Doob h -transformation, the generator for conditioned process Z_t is

$$(3.2) \quad Q^q f = \frac{1}{q} Q(qf) = Qf + \frac{2\varepsilon \nabla q}{q} \cdot \nabla f.$$

Since $q = 0$ in \bar{A} , a singular drift term prevents Z_t hitting A and also pushes $Z_t \in \partial A$ into $(\overline{A \cup B})^c$. For the delicate case Z_0 starting from ∂A with an appropriate initial law on ∂A , [LN15, Theorem 1.2] proved that the conditioned process Z_t with the augmented filtration is same in law as the k -th transition path process exiting from A then hitting B defined in [EVE06, MSVE06, EVE10]. More precisely, the initial and end distribution for Z_t , a.k.a. reactive exit and entrance distribution ν_0, ν_1 , can be calculated by the Dirichlet to Neumann map of the elliptic equation for committor function (3.1) [LN15, Proposition 1.5].

In Section 3.2, we will prove the resulting conditioned process (the transition path process) Z_t can be regarded as the original process with an additional control $\mathbf{v} = \frac{2\varepsilon \nabla q}{q}$. This control, indeed optimal control, together with the original landscape U , leads to an effective potential $U^e := U - 2\varepsilon \ln q$, which is $+\infty$ for $\mathbf{y} \in \bar{A}$ and U for $\mathbf{y} \in \bar{B}$. This effective potential guides the associated SDE of \tilde{Y}_t to the basin B before hitting A .

3.1.3. *Density and current of transition paths.* Next, using the conditioned process Z_t , which is also the controlled process \tilde{Y}_t in (3.15), and its generator Q^q , we sketch the derivation of the current of transition paths. Recall the equilibrium density of the original Markov process Y_t is $\pi \propto e^{-\frac{U}{\varepsilon}}$. From [LN15, Proposition 1.9][EVE06, Proposition 2], the density of transition paths is

$$(3.3) \quad \rho_R(\mathbf{y}) = \pi(\mathbf{y})q(\mathbf{y})(1 - q(\mathbf{y})).$$

Then some elementary calculations show that

$$(3.4) \quad (Q^q)^* \rho_R(\mathbf{y}) = 0, \quad \mathbf{y} \in (\overline{A \cup B})^c.$$

From (3.2) and (4.5),

$$(3.5) \quad 0 = (Q^q)^* \rho_R = Q^* \rho_R - \nabla \cdot \left(\rho_R \frac{2\varepsilon \nabla q}{q} \right) = \varepsilon \nabla \cdot \left(\pi \nabla \frac{\rho_R}{\pi} - \rho_R \frac{2\nabla q}{q} \right).$$

This divergence form, together with (3.3), gives the current of transition paths from A to B (upto a factor ε)

$$(3.6) \quad J_R := -\pi \nabla \frac{\rho_R}{\pi} + \rho_R \frac{2\nabla q}{q} = -\pi \nabla [q(1 - q)] + 2\pi(1 - q)\nabla q = \pi \nabla q.$$

One can also directly verify there is another equilibrium, besides ρ^R , such that $(Q^q)^* \pi^e = 0$

$$(3.7) \quad \pi^e := e^{-\frac{U^e}{\varepsilon}} = \pi q^2,$$

which vanishes at A .

3.2. Stochastic optimal control interpretation of the committor function. In this subsection, we will prove that the committor function q gives a stochastic optimal control such that the controlled Markov process realizes the transition from A to B with minimum running and terminal cost. We will first illustrate the idea of optimal change of measure in an abstract measurable space, then prove the stochastic optimal control interpretation in Theorem 3.2.

3.2.1. Duality between the relative entropy and the Helmholtz free energy. It is well known that the canonical ensemble is closely related to the optimal change of measure for the Helmholtz free energy. More precisely, let (Ω, \mathcal{F}) be a measurable space and $\mathbb{P}(\Omega)$ is the family of probability measures on Ω . Denote Hamiltonian $H \in \mathbb{R}$ as a measurable function on Ω . For a reference measure (a.k.a. prior measure) $P \in \mathbb{P}(\Omega)$, we define the Helmholtz free energy of Hamiltonian H with respect to P as

$$(3.8) \quad F(H) := -\frac{1}{\beta} \ln \left(\int_{\Omega} e^{-\beta H(\omega)} dP(\omega) \right) \in [-\infty, +\infty).$$

For any other measure $\tilde{P} \in \mathbb{P}(\Omega)$ which is absolutely continuous w.r.t. P , denote $\text{KL}(\tilde{P}|P) = \int_{\Omega} \ln \left(\frac{d\tilde{P}}{dP} \right) d\tilde{P}$ the relative entropy with respect to P . Then we have the following Legendre-type transformations and duality in statistical mechanics; c.f. [DS01].

(i) For any measure $\tilde{P} \ll P$

$$(3.9) \quad -\frac{1}{\beta} \text{KL}(\tilde{P}|P) = \sup_H \left\{ \int_{\Omega} H(\omega) d\tilde{P}(\omega) - F(H) \right\};$$

(ii) for any function $H(\omega)$

$$(3.10) \quad F(H) = \inf_{\tilde{P} \ll P} \left\{ \int_{\Omega} H(\omega) d\tilde{P}(\omega) + \frac{1}{\beta} \text{KL}(\tilde{P}|P) \right\} = \inf_{\tilde{P} \ll P} \left\{ \int_{\Omega} \left(H(\omega) + \frac{1}{\beta} \ln \frac{d\tilde{P}(\omega)}{dP(\omega)} \right) d\tilde{P}(\omega) \right\}.$$

In Theorem 3.2 later, we will use the second Legendre-type transformation (ii) for probability measures (induced by coordinate processes) on path space $\Omega = C([0, +\infty); \mathcal{N})$ to prove the optimality. To show the idea of the proof, if $dP = \rho_0 dx$ and $d\tilde{P} = \rho dx$, the optimal density ρ^* in the transformation is achieved when

$$(3.11) \quad e^{-\beta H - 1 + \lambda} = \frac{\rho^*}{\rho_0}, \quad \int \rho^* = 1 = e^{\lambda - 1} \int e^{-\beta H} \rho_0 dx,$$

where λ is the Lagrange multiplier to ensure ρ is a probability density. Then we have

$$(3.12) \quad \int H \rho^* dx + \frac{1}{\beta} \int \ln \frac{\rho^*}{\rho_0} \rho^* dx = \frac{\lambda - 1}{\beta} = F(H).$$

3.2.2. Optimal control with terminal cost. Now we give a theorem on the optimality of the control $\mathbf{v} = \frac{2\varepsilon \nabla q}{q} = 2\varepsilon \nabla \ln q$, which drives \mathbf{y} to B before hitting A .

Theorem 3.2. Assume the original Markov process Y_t has generator $Qf = \varepsilon \Delta f - \nabla U \cdot \nabla f$, $\varepsilon > 0$. The forward committor function q in (3.1) gives an optimal control $\mathbf{v}^* = \frac{2\varepsilon \nabla q}{q}$ in the sense that it drives the controlled process \tilde{Y}_t starting from $\mathbf{y} \in (\overline{A \cup B})^c$ to the set B before hitting A with the least action in (3.15). Moreover, the optimal control \mathbf{v}^* leads to an effective potential $U^e := U - 2\varepsilon \ln q$ for the controlled Markov process \tilde{Y}_t with the generator Q^q defined in (3.2).

Proof. Choose $\Omega = C([0, +\infty); \mathcal{N})$, with the product σ -algebra, as our measurable space [Var07]. Any element $\mathbf{y} \in \Omega$ gives a coordinate process $Y_t(\mathbf{y}) := \mathbf{y}(t) \in \mathcal{N}$, $t \geq 0$.

First, for the stopping time $\tau := \inf\{t \geq 0; Y_t \in \overline{A \cup B}\}$, from [Eva13, Section 6.2.1], the stochastic characterization of committor function q in (3.1) can be expressed as

$$(3.13) \quad q(\mathbf{y}) = \mathbb{E}_P(f(Y_\tau))$$

with function $f(\mathbf{z})$ on $\overline{A \cup B}$, $f = 0$, $\mathbf{z} \in \bar{A}$ while $f = 1$, $\mathbf{z} \in \bar{B}$. Here the expectation is taken under the probability measure P (called reference measure) on the path space Ω associated with all realizations of the original SDE of Y_t starting from $\mathbf{y} \in (\overline{A \cup B})^c$. Define $\beta := \frac{1}{2\varepsilon}$ and function

$$(3.14) \quad g := -\frac{1}{\beta} \ln f = \begin{cases} +\infty, & \text{in } \bar{A}; \\ 0, & \text{in } \bar{B}. \end{cases}$$

Then choose Hamiltonian $H(\mathbf{y}) := g(Y_\tau(\mathbf{y}))$ for $\mathbf{y} \in \Omega$. Since the original SDE for Y_t is translation invariant with respect to time (stationary w.r.t. time), so the control function $\mathbf{v}(Y_t)$ (stationary Markov control) does not explicitly depend on t and we can take the starting time as $t = 0$ without loss of generality. We consider the optimal control problem

$$(3.15) \quad \begin{aligned} \gamma(\mathbf{y}) &:= \min_{\mathbf{v} \in \mathcal{A}} \mathbb{E}_P \left[\int_0^\tau \frac{1}{2} |\mathbf{v}(\tilde{Y}_s)|^2 ds + g(\tilde{Y}_\tau) \right] \\ \text{s. t. } d\tilde{Y}_t &= (-\nabla U(\tilde{Y}_t) + \mathbf{v}(\tilde{Y}_t)) dt + \sqrt{2\varepsilon} d\mathcal{N}B_t, \quad \tilde{Y}_0 = \mathbf{y}, \end{aligned}$$

where $\mathbf{y} \in (\overline{A \cup B})^c$, τ is the stopping time associated with \tilde{Y}_t and the admissible control belongs to

$$(3.16) \quad \mathcal{A} := \{\mathbf{v} \in T_{\mathcal{N}}; \mathbb{E}_P \left(e^{\beta \int_0^\tau \frac{1}{2} |\mathbf{v}(\tilde{Y}_s)|^2 ds} \right) < \infty\}.$$

This condition is given by the well known Novikov condition in the Girsanov's transformation, which ensures the almost sure positivity of the Radon-Nikodym derivative in (3.18). It is easy to see $\mathbf{v} = 0$ belongs to \mathcal{A} so $\mathcal{A} \neq \emptyset$. However from the definition of g , $g(Y_\tau) = +\infty$ when $Y_\tau \in \bar{A}$, so $\mathbf{v} = 0$ is not an optimal control. We also remark that the selection effect due to g , i.e. the controlled system will hit B before A , can be equivalently added to the admissible control set (3.16).

Second, we find the minimizer γ (a.k.a value function) and the corresponding optimal control \mathbf{v}^* . Let \tilde{P} be the probability measure on Ω associated with all realizations of the SDE of \tilde{Y}_t with control \mathbf{v} . By the Girsanov's theorem, Y_t is a Brownian motion under measure P and \tilde{Y}_t is a Brownian motion under measure \tilde{P} . As a consequence,

$$(3.17) \quad \mathbb{E}_P(e^{-\beta g(Y_\tau)}) = \mathbb{E}_{\tilde{P}}(e^{-\beta g(\tilde{Y}_\tau)}) = \mathbb{E}_P \left(e^{-\beta g(\tilde{Y}_\tau)} \frac{d\tilde{P}}{dP} \right),$$

where the Radon-Nikodym derivative is given by [Var07, Theorem 6.2]

$$(3.18) \quad \frac{d\tilde{P}}{dP} = e^{-\beta \int_0^\tau \sqrt{2\varepsilon} \mathbf{v}(\tilde{Y}_s) \cdot d\mathcal{N}B_s - \frac{\beta}{2} \int_0^\tau |\mathbf{v}(\tilde{Y}_s)|^2 ds} > 0, \quad P\text{-a.s.}$$

and the sign in front of $d\mathcal{N}B$ is negative following the convention. In short, we have

$$(3.19) \quad \mathbb{E}_P(e^{-\beta H(\mathbf{y})}) = \mathbb{E}_P(e^{-\beta g(Y_\tau)}) = \mathbb{E}_P \left(e^{-\beta \left(g(\tilde{Y}_\tau) + \int_0^\tau \sqrt{2\varepsilon} \mathbf{v}(\tilde{Y}_s) \cdot d\mathcal{N}B_s + \frac{1}{2} \int_0^\tau |\mathbf{v}(\tilde{Y}_s)|^2 ds \right)} \right).$$

Then by Jensen's inequality,

$$(3.20) \quad e^{-\beta \mathbb{E}_P(g(\tilde{Y}_\tau) + \int_0^\tau \frac{1}{2} |\mathbf{v}(\tilde{Y}_s)|^2 ds)} \leq \mathbb{E}_P \left(e^{-\beta g(\tilde{Y}_\tau)} \frac{d\tilde{P}}{dP} \right).$$

Here the equality is achieved if and only if $g(\tilde{Y}_\tau) + \int_0^\tau \sqrt{2\varepsilon} \mathbf{v}(\tilde{Y}_s) \cdot d\mathcal{N}B_s + \int_0^\tau \frac{1}{2} |\mathbf{v}(\tilde{Y}_s)|^2 ds$ is deterministic. Taking the logarithm to both sides, we have

$$(3.21) \quad \mathbb{E}_P \left(g(\tilde{Y}_\tau) + \int_0^\tau \frac{1}{2} |\mathbf{v}(\tilde{Y}_s)|^2 ds \right) \geq -\frac{1}{\beta} \ln \left(\mathbb{E}_P \left(e^{-\beta g(\tilde{Y}_\tau)} \frac{d\tilde{P}}{dP} \right) \right) = -\frac{1}{\beta} \ln \left(\mathbb{E}_P(e^{-\beta g(Y_\tau)}) \right),$$

which, together with (3.13), gives

$$(3.22) \quad \gamma(\mathbf{y}) \geq -\frac{1}{\beta} \ln \left(\mathbb{E}_P(e^{-\beta g(Y_\tau)}) \right) = -\frac{1}{\beta} \ln \left(\mathbb{E}_P(f(Y_\tau)) \right) = -\frac{1}{\beta} \ln q(\mathbf{y}).$$

Furthermore, the verification theorem [FS06, IV.3, Theorem 5.1] shows that the equality is indeed achieved $\gamma(\mathbf{y}) = -\frac{1}{\beta} \ln q(\mathbf{y})$. Actually, $\gamma(\mathbf{y})$ satisfies the Hamilton-Jacobi-Bellman equation

$$(3.23) \quad \varepsilon \Delta \gamma - \frac{1}{2} |\nabla \gamma|^2 - \nabla U \cdot \nabla \gamma = 0, \quad \text{in } (\overline{A \cup B})^c, \quad \gamma = g \quad \text{on } \overline{A \cup B}.$$

The associated optimal control (optimal feedback), such that

$$(3.24) \quad \tilde{H}(\mathbf{y}) := g(\tilde{Y}_\tau) + \int_0^\tau \sqrt{2\varepsilon} \mathbf{v}^*(\tilde{Y}_s) \cdot d\mathcal{N}B_s + \int_0^\tau \frac{1}{2} |\mathbf{v}^*(\tilde{Y}_s)|^2 ds$$

being deterministic, is given by

$$(3.25) \quad \mathbf{v}^* = -\nabla \gamma = \frac{1}{\beta} \nabla \ln \mathbb{E}_P \left(e^{-\beta g(Y_\tau)} \right) = \frac{1}{\beta} \nabla \ln q.$$

Indeed, one can verify this by applying Ito's formula to $\gamma(\tilde{Y}_\tau)$

$$(3.26) \quad \begin{aligned} I_1 &:= \gamma(\tilde{Y}_\tau) - \gamma(\tilde{Y}_0) = 1 - \gamma(\mathbf{y}) \\ &= \int_0^\tau \tilde{Q}\gamma(\tilde{Y}_s) ds + \sqrt{2\varepsilon} \int_0^\tau \nabla \gamma \cdot d\mathcal{N}B_s \\ &= \int_0^\tau \varepsilon \Delta \gamma(\tilde{Y}_s) + (-\nabla U + \mathbf{v}) \cdot \nabla \gamma(\tilde{Y}_s) ds + \sqrt{2\varepsilon} \int_0^\tau \nabla \gamma \cdot d\mathcal{N}B_s \\ &= \int_0^\tau (\varepsilon \Delta \gamma - \nabla U \cdot \nabla \gamma - |\nabla \gamma|^2)(\tilde{Y}_s) ds + \sqrt{2\varepsilon} \int_0^\tau \nabla \gamma \cdot d\mathcal{N}B_s \\ &= -\frac{1}{2} \int_0^\tau |\nabla \gamma|^2(\tilde{Y}_s) ds + \sqrt{2\varepsilon} \int_0^\tau \nabla \gamma \cdot d\mathcal{N}B_s, \end{aligned}$$

where \tilde{Q} is the generator of \tilde{Y}_t and we used $\mathbf{v}^* = -\nabla \gamma$ and (3.23). On the other hand,

$$(3.27) \quad \begin{aligned} I_2 &:= \int_0^\tau \sqrt{2\varepsilon} \mathbf{v}^*(\tilde{Y}_s) \cdot d\mathcal{N}B_s + \int_0^\tau \frac{1}{2} |\mathbf{v}^*(\tilde{Y}_s)|^2 ds \\ &= -\sqrt{2\varepsilon} \int_0^\tau \nabla \gamma \cdot d\mathcal{N}B_s + \frac{1}{2} \int_0^\tau |\nabla \gamma|^2 ds \end{aligned}$$

due to $\mathbf{v}^* = -\nabla \gamma$. Then we have

$$(3.28) \quad I_1 + I_2 = \int_0^\tau \left(\varepsilon \Delta \gamma - \frac{1}{2} |\nabla \gamma|^2 - \nabla U \cdot \nabla \gamma \right) ds = 0,$$

which, together with $I_1 = 1 - \gamma(\mathbf{y})$, shows \tilde{H} is deterministic. Since the optimality ensures \tilde{H} in (3.24) is deterministic, so

$$\mathbb{E}_P \left(e^{-\beta \tilde{H}} \right) = e^{-\mathbb{E}_P(\beta \tilde{H})} = e^{\mathbb{E}_P(\beta I_1)} = e^{\beta(1-\gamma)} = qe^\beta < +\infty$$

and thus $\mathbf{v}^* \in \mathcal{A}$.

Finally, plugging the optimal control $\mathbf{v}^* = 2\varepsilon \nabla \ln q$ into (3.15) shows the effective potential for the controlled Markov process \tilde{Y}_t is

$$(3.29) \quad U^e = U - 2\varepsilon \ln q.$$

Then by Ito's formula, the master equation for the controlled Markov process \tilde{Y}_t is

$$(3.30) \quad \partial_t \rho = \varepsilon \nabla \cdot \left(e^{-\frac{U^e}{\varepsilon}} \nabla (\rho e^{\frac{U^e}{\varepsilon}}) \right) = \varepsilon \nabla \cdot \left(\pi^e \nabla \frac{\rho}{\pi^e} \right).$$

□

Remark 3.3. *We remark Theorem 3.2 uses a terminal cost function g and the associated committor function q to construct an optimal feedback \mathbf{v}^* and thus the associated controlled process \tilde{Y} . More importantly, the transition from stable basin A to another basin B is a rare event for the original Markov process Y_t while this transition becomes an almost sure event for the controlled Markov process \tilde{Y}_t . This has significant statistic advantage because using the controlled process \tilde{Y}_t , which realizes the conformational transitions almost surely. The computations for statistic quantities in the original rare event becomes more efficient; see the Algorithm 4 for the controlled random walk on point clouds.*

4. MARKOV PROCESS AND TRANSITION PATH THEORY ON POINT CLOUDS

This section focuses on constructing an approximated Markov process on point clouds and computing the discrete analogies in the transition path theory on point clouds. In Section 4.1, we will first introduce the upwind scheme which approximates the original Langevin dynamics (1.1) and its master equation on \mathcal{N} . In Section 4.2, based on the approximated Markov process, we design the discrete counterparts for the committor functions, the effective Doob h -transformation, the generator for the optimal controlled Markov process in the transition path theory on point clouds.

4.1. Upwind scheme and the approximated Markov process on point clouds. In this section, we first propose an upwind scheme for the original Fokker-Planck equation based on a data-driven approximated Voronoi tessellation for \mathcal{N} . Then we reformulate it as a Markov process on point clouds.

4.1.1. Voronoi tessellation and upwind scheme. Suppose $(\mathcal{N}, d_{\mathcal{N}})$ is a d dimensional smooth closed submanifold of \mathbb{R}^ℓ and $d_{\mathcal{N}}$ is induced by the Euclidean metric in \mathbb{R}^ℓ . $D := \{\mathbf{y}_i\}_{i=1:n}$ are point clouds sampled from some density on \mathcal{N} bounded below and above. It is proved that the data points D are well-distributed on \mathcal{N} whenever the points are sampled from a density function with lower and upper bounds [TS15, LLL19]. Define the Voronoi cell as

$$(4.1) \quad C_i := \{\mathbf{y} \in \mathcal{N}; d_{\mathcal{N}}(\mathbf{y}, \mathbf{y}_i) \leq d_{\mathcal{N}}(\mathbf{y}, \mathbf{y}_j) \text{ for all } \mathbf{y}_j \in D\} \quad \text{with volume } |C_i| = \mathcal{H}^d(C_i).$$

Then $\mathcal{N} = \bigcup_{i=1}^n C_i$ is a Voronoi tessellation of \mathcal{N} . Denote the Voronoi face for cell C_i as

$$(4.2) \quad \Gamma_{ij} := C_i \cap C_j \text{ with its area } |\Gamma_{ij}| = \mathcal{H}^{d-1}(\Gamma_{ij}),$$

for any $j = 1, \dots, n$. If $\Gamma_{ij} = \emptyset$ or $i = j$ then we set $|\Gamma_{ij}| = 0$. Define the associated adjacent sample points as

$$(4.3) \quad VF(i) := \{j; \Gamma_{ij} \neq \emptyset\}.$$

By Ito's formula, SDE (1.1) gives the following Fokker-Planck equation, which is the master equation for the density $\rho(\mathbf{y})$ in terms of \mathbf{y} ,

$$(4.4) \quad \partial_t \rho = \nabla \cdot (\varepsilon \nabla \rho + \rho \nabla U) =: FP^\mathcal{N} \rho.$$

Denote the equilibrium $\pi := e^{-\frac{U}{\varepsilon}}$. The Fokker-Planck operator has the following equivalent form

$$(4.5) \quad \begin{aligned} FP^\mathcal{N}(\rho) &= \varepsilon \Delta \rho + \nabla \cdot (\rho \nabla U) = \nabla \cdot (\rho (\varepsilon \nabla \ln \rho + \nabla U)) \\ &= \varepsilon \nabla \cdot \left(\rho \nabla \ln \frac{\rho}{\pi} \right) = \varepsilon \nabla \cdot \left(\pi \nabla \frac{\rho}{\pi} \right). \end{aligned}$$

Using (4.5) and the finite volume method, we have an upwind scheme

$$(4.6) \quad \frac{d}{dt} \rho_i |C_i| = \frac{1}{2} \sum_{j \in VF(i)} \frac{\pi_i + \pi_j}{|y_i - y_j|} |\Gamma_{ij}| \left(\frac{\rho_j}{\pi_j} - \frac{\rho_i}{\pi_i} \right), \quad i = 1, \dots, n,$$

where π_i is the approximated equilibrium density at \mathbf{y}_i with the volume element $|C_i|$. With an adjoint Q -matrix, we rewrite (4.6) in the operator form

$$(4.7) \quad \frac{d}{dt} \rho |C| = Q^*(\rho |C|) \quad \text{with } \rho |C| = \{\rho_i |C_i|\}_{i=1:n};$$

see (4.13) for the explicit componentwise expression for the Q -matrix. If ρ_i is an approximation of the density $\rho(\mathbf{y}_i)$, then the piecewise constant density $\rho^{\text{approx}}(\mathbf{y}) := \sum_i \rho_i \chi_{C_i}(\mathbf{y})$ is an approximation of density $\rho(\mathbf{y})$. One can also recast (4.6) as a backward equation formulation

$$(4.8) \quad \frac{d}{dt} \frac{\rho_i}{\pi_i} = \sum_{j \in VF(i)} \frac{\pi_i + \pi_j}{2\pi_i |C_i| |y_i - y_j|} |\Gamma_{ij}| \left(\frac{\rho_j}{\pi_j} - \frac{\rho_i}{\pi_i} \right), \quad i = 1, \dots, n.$$

Equivalently, with the constructed Q -matrix, we rewrite (4.8) in the operator form

$$(4.9) \quad \frac{d}{dt} \frac{\rho}{\pi} = Q \frac{\rho}{\pi} \quad \text{with } \frac{\rho}{\pi} = \left(\frac{\rho_i}{\pi_i} \right)_{i=1:n}.$$

In practice, since we don't have the exact manifold information, the volume of the Voronoi cells C_k and the area of the Voronoi faces Γ_{kl} need to be approximated using Algorithm 1 in Section 5. We denote the approximated volumes as $|\tilde{C}_k|$ and the approximated areas as $|\tilde{\Gamma}_{kl}|$. After replacing C_k by the approximated volumes $|\tilde{C}_k|$ and replacing Γ_{kl} by the approximated areas $|\tilde{\Gamma}_{kl}|$, (4.6)/ (4.10) becomes an approximated Markov process on point clouds, which is an implementable solver for the Fokker-Planck equation on \mathcal{N} . We refer to [GLW20] for the convergence analysis of this solver (4.6) for the Fokker-Planck equation (4.4). We drop tildes without confusion in the following contexts.

4.1.2. Markov process on point clouds. With the approximated volumes $|C_i|$ and the approximated areas $|\Gamma_{ij}|$, one can interpret the upwind scheme (4.6) as the forward equation for a Markov process with transition probability P_{ji} (from j to i) and jump rate λ_j

$$(4.10) \quad \frac{d}{dt} \rho_i |C_i| = \sum_{j \in VF(i)} \lambda_j P_{ji} \rho_j |C_j| - \lambda_i \rho_i |C_i|, \quad i = 1, 2, \dots, n,$$

where

$$(4.11) \quad \begin{aligned} \lambda_i &:= \frac{1}{2|C_i|\pi_i} \sum_{j \in VF(i)} \frac{\pi_i + \pi_j}{|y_i - y_j|} |\Gamma_{ij}|, \quad i = 1, 2, \dots, n; \\ P_{ji} &:= \frac{1}{\lambda_j} \frac{\pi_i + \pi_j}{2\pi_j|C_j|} \frac{|\Gamma_{ij}|}{|y_i - y_j|}, \quad j \in VF(i); \quad P_{ji} = 0, \quad j \notin VF(i). \end{aligned}$$

Assume $\pi_i > 0$ for all i , then we have $\lambda_i > 0$ for all i . One can see it satisfies $\sum_i P_{ji} = 1$ and the detailed balance property

$$(4.12) \quad P_{ji}\lambda_j\pi_j|C_j| = P_{ij}\lambda_i\pi_i|C_i|.$$

Define Q as the matrix

$$(4.13) \quad Q_{ij} = \begin{cases} -\lambda_i, & j = i, \\ \lambda_i P_{ij}, & j \neq i. \end{cases}$$

Notice $\sum_j Q_{ij} = 0$. Then Q is the generator of the associated Markov process.

4.2. Committor function, currents, and controlled Markov process on point clouds.

In this section, we first review the corresponding concepts for the transition path theory on point clouds. Then from the optimal control viewpoint, we construct the upwind scheme for the controlled Fokker-Planck equation and the associated controlled Markov process (random walk on point clouds).

4.2.1. Committor function, currents, and transition rate. Suppose the local minimums a, b of U are two cell center with index i_a and i_b . Below, we clarify the discrete counterparts of Section 3.1 for committor functions q , the density of transition paths ρ_R , the current of transition paths J_R and the transition rates k_{AB} .

First, from the backward equation formulation (4.8), the forward committor function q_i , $i = 1, \dots, n$ from a to b satisfies

$$(4.14) \quad \begin{aligned} \sum_{j \in VF(i)} \frac{\pi_i + \pi_j}{2\pi_i|C_i||y_i - y_j|} |\Gamma_{ij}| (q_j - q_i) &= 0, \quad i \neq i_a, i_b, \\ q_{i_a} &= 0, \quad q_{i_b} = 1. \end{aligned}$$

Second, the discrete density of the reactive path [MSVE09, Remark 2.10] is defined as

$$(4.15) \quad \rho_i^R := \pi_i q_i (1 - q_i).$$

Third, with the constructed Q -matrix in (4.13), the current from site i to site j of the reactive path from state a to state b is given by [MSVE09, Remark 2.17]

$$(4.16) \quad J_{ij}^R := Q_{ij}\pi_i(q_j - q_i) = \frac{(\pi_i + \pi_j)|\Gamma_{ij}|}{2} \frac{q_j - q_i}{|y_i - y_j|},$$

which is the counterpart of the current in (3.6). Due to (4.14), it is easy to check the current is divergence free, i.e., satisfying the Kirchhoff's current law,

$$(4.17) \quad \sum_{j \in VF(i)} J_{ij}^R = 0, \quad i \neq i_a, i_b.$$

Finally, the transition rate from stable basin A to basin B can be calculated by current. It is shown in [MSVE09, Theorem 2.15] that the transition rate from A to B is given by

$$(4.18) \quad k_{AB} = \sum_{i \in A} \sum_{j=1}^n J_{ij}^R.$$

Particularly, if there is only one point $\mathbf{y}_{i_a} \in A$, then

$$(4.19) \quad k_{AB} = \langle Qq, \delta_{i_a} \rangle_\pi = \sum_{j \in VF(i_a)} J_{i_a, j}^R,$$

where δ_{i_a} is the Kronecker delta with value 1 if $i = i_a$ while 0 otherwise.

4.2.2. Upwind scheme and Q^q -matrix for controlled Markov process. Similar to the controlled Markov process in (3.30), we give the controlled Markov process on point clouds below. Suppose the local minimums a, b of U are two cell center with index i_a, i_b and for simplicity we assume there is only one point $\mathbf{y}_{i_a} \in \bar{A}$. We construct a controlled random walk on point clouds $\{\mathbf{y}_i\}_{i=1:n, i \neq i_a}$. The controlled random walk for the general case that more than one point belong to A is similar.

First, with the effective potential U^e in (3.29), the effective equilibrium is $\pi^e = e^{-\frac{U^e}{\varepsilon}} = q^2 \pi$. Then we plug $\pi_i^e := q_i^2 \pi_i$ into the upwind scheme (4.6). Thus we propose an upwind scheme for the controlled Fokker-Planck equation (3.30)

$$(4.20) \quad \frac{d}{dt} \rho_i |C_i| = \frac{1}{2} \sum_{j \in VF(i), j \neq i_a} \frac{q_i q_j (\pi_i + \pi_j)}{|y_i - y_j|} |\Gamma_{ij}| \left(\frac{\rho_j}{q_j^2 \pi_j} - \frac{\rho_i}{q_i^2 \pi_i} \right), \quad i = 1, \dots, n, \quad i \neq i_a.$$

With the notation $\rho|C| = \{\rho_i |C_i|\}_{i=1:n, i \neq i_a}$, (4.20) can be recast as the vector formulation

$$(4.21) \quad \frac{d}{dt} \rho|C| = (Q^q)^*(\rho|C|),$$

where Q^q is the effective generator for the controlled Markov process; see specific matrix in (4.27). One can also recast (4.20) as a backward equation

$$(4.22) \quad \frac{d}{dt} \frac{\rho_i}{\pi_i^e} = \frac{1}{2} \sum_{j \in VF(i), j \neq i_a} \frac{q_j}{q_i} \frac{(\pi_i + \pi_j)}{|C_i| \pi_i |y_i - y_j|} |\Gamma_{ij}| \left(\frac{\rho_j}{\pi_j^e} - \frac{\rho_i}{\pi_i^e} \right), \quad i = 1, \dots, n, \quad i \neq i_a,$$

which in the vector form is

$$(4.23) \quad \frac{d}{dt} \frac{\rho}{\pi^e} = Q^q \left(\frac{\rho}{\pi^e} \right).$$

On the one hand, it is easy to see π^e is one equilibrium to the controlled random walk with generator Q^q . On the other hand, there is another equilibrium ρ^R defined in (4.15). Indeed, we plug ρ_i^R into (4.20) and check it is still the equilibrium for the controlled Markov process. Using (4.14), we have

$$(4.24) \quad \frac{1}{2} \sum_{j \in VF(i), j \neq i_a} \frac{q_i q_j (\pi_i + \pi_j)}{|y_i - y_j|} |\Gamma_{ij}| \left(\frac{1}{q_j} - \frac{1}{q_i} \right) = -\frac{1}{2} \sum_{j \in VF(i), j \neq i_a} \frac{\pi_i + \pi_j}{|y_i - y_j|} |\Gamma_{ij}| (q_i - q_j) = 0, \\ i = 1, \dots, n, \quad i \neq i_a.$$

Thus there is no spectral gap for the controlled generator Q^q since the principal eigenvalue has at least two eigenvectors π^e and ρ^R .

Next, one can recast (4.22) as the controlled Markov process with the controlled transition probability P_{ji}^q (from site j to i) and the controlled jump rate λ_j^q

$$(4.25) \quad \frac{d}{dt} \rho_i |C_i| = \sum_{j \in VF(i), j \neq i_a} \lambda_j^q P_{ji}^q \rho_j |C_j| - \lambda_i^q \rho_i |C_i|, \quad i = 1, 2, \dots, n, \quad i \neq i_a,$$

where

$$(4.26) \quad \lambda_i^q = \frac{1}{2|C_i|\pi_i} \sum_{j \in VF(i), j \neq i_a} \frac{q_j}{q_i} \frac{\pi_i + \pi_j}{|y_i - y_j|} |\Gamma_{ij}|, \quad i = 1, 2, \dots, n, \quad i \neq i_a;$$

$$P_{ji}^q = \frac{1}{\lambda_j^q} \frac{q_i}{q_j} \frac{\pi_i + \pi_j}{2\pi_j |C_j|} \frac{|\Gamma_{ij}|}{|y_i - y_j|}, \quad j \in VF(i), j \neq i_a; \quad P_{ji}^q = 0, \quad j \notin VF(i).$$

Then Q^q can be explicitly recast as the matrix

$$(4.27) \quad Q_{ij}^q = \begin{cases} -\lambda_i^q, & j = i, \\ \lambda_i^q P_{ij}^q, & j \neq i, \end{cases} \quad i, j = 1, 2, \dots, n, \quad i, j \neq i_a.$$

With the constructed controlled transition probability P_{ji}^q for the controlled random walk, we will provide an alternative algorithm for finding the minimum energy path from A to B . The minimum energy path is the most probable path, which is usually assumed to be closed to the average path. Thus the minimum energy path can be simulated by the Monte Carlo method for the controlled random walk on point clouds; see Algorithm 5.

Remark 4.1. *Similar to the continuous version, we calculate the Doob h -transformation and recast the effective generator for the controlled Markov process. From (4.20),*

$$(4.28) \quad \begin{aligned} \frac{d}{dt} \rho_i |C_i| &= (Q^q)^*(\rho |C|) := \frac{1}{2} \sum_{j \in VF(i)} \frac{(\pi_i + \pi_j)}{|y_i - y_j|} |\Gamma_{ij}| \left(\frac{q_i}{q_j} \frac{\rho_j}{\pi_j} - \frac{q_j}{q_i} \frac{\rho_i}{\pi_i} \right) \\ &= \frac{1}{2} \sum_{j \in VF(i)} \frac{(\pi_i + \pi_j)}{|y_i - y_j|} |\Gamma_{ij}| \left(\frac{\rho_j}{\pi_j} - \frac{\rho_i}{\pi_i} + \left(\frac{q_i}{q_j} - 1 \right) \frac{\rho_j}{\pi_j} - \left(\frac{q_j}{q_i} - 1 \right) \frac{\rho_i}{\pi_i} \right) \\ &= \frac{1}{2} \sum_{j \in VF(i)} \frac{(\pi_i + \pi_j)}{|y_i - y_j|} |\Gamma_{ij}| \left(\frac{\rho_j}{\pi_j} - \frac{\rho_i}{\pi_i} \right) + \frac{1}{2} \sum_{j \in VF(i)} \frac{(\pi_i + \pi_j)}{|y_i - y_j|} |\Gamma_{ij}| \left(\frac{\rho_j}{q_j \pi_j} + \frac{\rho_i}{q_i \pi_i} \right) (q_i - q_j) \\ &= Q^*(\rho |C|) - \sum_{j \in VF(i)} |\Gamma_{ij}| \frac{q_j - q_i}{|y_i - y_j|} \frac{(\pi_i + \pi_j)}{2} \left(\frac{\rho_j}{q_j \pi_j} + \frac{\rho_i}{q_i \pi_i} \right) \\ &= Q^*(\rho |C|) - \sum_{j \in VF(i)} |\Gamma_{ij}| v_{ij} \rho_{ij}, \end{aligned}$$

where $v_{ij} = 2 \frac{(q_j - q_i)}{|y_j - y_i|} \frac{2}{q_i + q_j}$ and $\rho_{ij} = \frac{1}{8} (q_i + q_j) (\pi_i + \pi_j) \left(\frac{\rho_j}{q_j \pi_j} + \frac{\rho_i}{q_i \pi_i} \right)$. This reformulation of the controlled generator Q^q can be regarded as the discrete counterpart of the generator in the Doob h -transformation (3.2). Thus, as a counterpart of Theorem 3.2, from the optimal control viewpoint for the Markov process (random walk) on point clouds, we can regard

$$(4.29) \quad v_{ij} = 2 \frac{(q_j - q_i)}{|y_j - y_i|} \frac{2}{q_i + q_j}$$

as the discrete optimal feedback control field from i to j (along edge e_{ij} of the associated Delaunay triangulation).

5. DATA-DRIVEN SOLVER AND COMPUTATIONS

In this section, based on the approximated (controlled) Markov process on points clouds, we introduce the detailed algorithms for finding the transition path on point clouds. Algorithm for the approximated Markov process is given in Section 5.1. Algorithms for the dominant transition path is given in Section 5.2. Algorithms for the Monte Carlo simulation and the mean transition path based on the controlled Markov process are given in Section 5.3. The corresponding numerical examples are conducted in Section 5.4.

5.1. Computation of the coefficients in the forward equation. We will first introduce the computations of the coefficients in the forward equation (4.14), i.e., the approximated cell volumes $|C_k|$ and the approximated edge areas $|\Gamma_{kl}|$, which are obtained by the approximated Voronoi tessellation in [GLW20]. Another related local meshed method for computing the committor function via point clouds is given in [LL18].

For bandwidth $0 < r < 1$ and $\mathbf{y}_k \in \{\mathbf{y}_i\}_{i=1:n}$, suppose that $\mathcal{B}_{\sqrt{r}}^{\mathbb{R}^\ell}(\mathbf{y}_k) \cap \{\mathbf{y}_i\}_{i=1:n} = \{\mathbf{y}_{k,1}, \dots, \mathbf{y}_{k,\bar{N}_k}\}$. We define the discrete local covariance matrix at \mathbf{y}_k ,

$$(5.1) \quad C_{n,r}(\mathbf{y}_k) := \frac{1}{n} \sum_{i=1}^{\bar{N}_k} (\mathbf{y}_{k,i} - \mathbf{y}_k)(\mathbf{y}_{k,i} - \mathbf{y}_k)^\top \in \mathbb{R}^{\ell \times \ell}.$$

Suppose $\{\beta_{n,r,1}, \dots, \beta_{n,r,d}\}$ are the first d orthonormal eigenvectors corresponding to $C_{n,r}(\mathbf{y}_k)$'s largest d eigenvalues. Define a map $\iota_k(u) : \mathbb{R}^\ell \rightarrow \mathbb{R}^d$ as

$$(5.2) \quad \iota_k(u) := (u^\top \beta_{n,r,1}, \dots, u^\top \beta_{n,r,d}).$$

For any $\mathbf{y} \in \mathbb{R}^\ell$, define $\tilde{\iota}_k(\mathbf{y}) = \iota_k(\mathbf{y} - \mathbf{y}_k)$. Based on the above definition, we summarize the approximated Voronoi tessellation in [GLW20] in Algorithm 1 to find the approximated volumes $|\tilde{C}_k|$ of the Voronoi cells C_k and the approximated areas $|\tilde{\Gamma}_{kl}|$ of the Voronoi faces Γ_{kl} .

Algorithm 1: Approximation of the Voronoi cell volumes and areas

Algorithm Inputs: Bandwidth r and the threshold s .

- 1 Choose $0 < r < 1$. For each $\mathbf{y}_k \in \{\mathbf{y}_i\}_{i=1}^n$, find

$$\mathcal{B}_{\sqrt{r}}^{\mathbb{R}^\ell}(\mathbf{y}_k) \cap \{\mathbf{y}_i\}_{i=1}^n =: \{\mathbf{y}_{k,1}, \dots, \mathbf{y}_{k,\bar{N}_k}\}, \quad \mathcal{B}_r^{\mathbb{R}^\ell}(\mathbf{y}_k) \cap \{\mathbf{y}_i\}_{i=1}^n =: \{\mathbf{y}_{k,1}, \dots, \mathbf{y}_{k,N_k}\}.$$

- 2 Construct $C_{n,r}(\mathbf{y}_k)$ as in (5.1) with $\{\mathbf{y}_{k,1}, \dots, \mathbf{y}_{k,\bar{N}_k}\}$. Find the orthonormal eigenvectors, denoted as $\{\beta_{n,r,1}, \dots, \beta_{n,r,d}\}$, corresponding to $C_{n,r}(\mathbf{y}_k)$'s largest d eigenvalues.
- 3 Use $\{\beta_{n,r,1}, \dots, \beta_{n,r,d}\}$ to construct $\tilde{\iota}_k$ as in (5.2). Find $v_{k,i} = \tilde{\iota}_k(\mathbf{y}_{k,i})$, for $i = 1, \dots, N_k$.
- 4 Find the Voronoi cell decomposition of $\{0, v_{k,1}, \dots, v_{k,N_k}\}$ in \mathbb{R}^d via Delaunay triangulation. Denote the Voronoi cell containing 0 to be $\tilde{C}_{k,0}$ and the Voronoi cell containing $v_{k,i}$ to be $\tilde{C}_{k,i}$. Denote the face $\tilde{F}_{k,i} = \tilde{C}_{k,0} \cup \tilde{C}_{k,i}$.
- 5 Find the approximation of $|C_k|$ as $|\tilde{C}_k| := |\tilde{C}_{k,0}| = \mathcal{H}^d(\tilde{C}_{k,0})$.
- 6 Find $|\tilde{F}_{k,i}| = \mathcal{H}^{d-1}(\tilde{F}_{k,i})$. Define $\tilde{\Gamma} \in \mathbb{R}^{n \times n}$ such that

$$(5.3) \quad A_{kl} := \frac{\tilde{A}_{kl} + \tilde{A}_{lk}}{2}, \quad \tilde{A}_{kl} = \begin{cases} |\tilde{F}_{k,i}| & \text{if } \mathbf{y}_l = \mathbf{y}_{k,i} \in B_r^{\mathbb{R}^\ell}(\mathbf{y}_k); \\ 0 & \text{otherwise.} \end{cases}$$

- 7 If $A_{kl} \geq s$, set $|\tilde{\Gamma}_{kl}| = A_{kl}$; otherwise $|\tilde{\Gamma}_{kl}| = s$. Then $|\tilde{\Gamma}_{kl}|$ is an approximation of $|\Gamma_{kl}|$.
-

5.2. Computation of dominant transition path. Based on the point clouds $\{\mathbf{y}_i\}_{i=1:n}$ and the associated Markov process (4.13) approximated in Section 5.1, we can compute the dominant transition path and the transition rate between metastable states on manifold \mathcal{N} . Let us first introduce the basic concepts and algorithms of the transition path theory of the Markov jump process in [MSVE09].

We seek the most probable path from the starting state A to the ending state B , so we construct a weighted directed graph $G(V, E)$ using dataset $V = \{\mathbf{y}_i\}_{i=1:n}$ as nodes, $E = \{e_{ij}, J_{ij}^R > 0\}$ as a directed edge with weight J_{ij}^R . Here $J_{ij}^R > 0$ is computed via (4.16). From (4.16), there is no loop in the directed graph $G(V, E)$.

Given the starting and ending states $A, B \subset \{\mathbf{y}_i\}_{i=1:n}$, a reactive trajectory from A to B is an ordered sequence $P = [\mathbf{y}_0, \mathbf{y}_1, \dots, \mathbf{y}_k]$, $\mathbf{y}_i \in V$, $(\mathbf{y}_i, \mathbf{y}_{i+1}) \in E$ such that $\mathbf{y}_0 \in A$, $\mathbf{y}_k \in B$ and $\mathbf{y}_i \in (A \cup B)^c$, $0 < i < k$ for some $k \leq n$. We denote the set of all such reactive trajectories by \mathcal{P} . From (4.16), along any reactive trajectory $P \in \mathcal{P}$, the values of the committor function

$$0 = q_0 < q_1 < \dots < q_k = 1$$

is strictly increasing from 0 to 1. Given a reactive trajectory P , the maximum flux carried by this reactive trajectory P , called capacity of P , is

$$c(P) := \min_{(i,j) \in P} J_{ij}^R.$$

Among all possible trajectories from A to B , one can further find the one with the largest capacity

$$(5.4) \quad c_{\max} := \max_{P \in \mathcal{P}} c(P), \quad P_{\max} \in \operatorname{argmax}_{P \in \mathcal{P}} c(P).$$

We call the associated edge

$$(5.5) \quad (b_1, b_2) = \operatorname{argmin}_{(i,j) \in P_{\max}} J_{ij}^R$$

the dynamical bottleneck with the weight $c_{\max} = J_{b_1 b_2}^R$. For simplicity, we assume J_{ij}^R are distinct, so b_1, b_2 are uniquely determined.

Finding the bottleneck provides a divide-and-conquer algorithm for finding the most probable path recursively. The dominant transition path is the reactive path with the largest effective probability current [MSVE09, EVE10]. Computing the dominant transition path is a recursion of finding the maximum capacity on subgraphs.

Now we use the bottleneck (b_1, b_2) and level-set of committor function q to divide the original graph $G(V, E)$ as two disconnected subgraphs G_L and G_R as below.

Note that every path in P_{\max} pass through the bottleneck (b_1, b_2) . Thus the weight of each edge in P_{\max} is larger than the weight of bottleneck $J_{b_1 b_2}^R$. So we first remove all the edges of the original graph $G(V, E)$ with weight smaller than $J_{b_1 b_2}^R$. Denote

$$(5.6) \quad V_L := \{\mathbf{y}_i; q_i \leq q_{b_1}\}, \quad V_R := \{\mathbf{y}_i; q_i \geq q_{b_2}\}.$$

Construct the new graph

$$(5.7) \quad \begin{aligned} G_L &:= (V_L, E_L), \quad \text{with } E_L := \{e_{ij} \in E; \mathbf{y}_i, \mathbf{y}_j \in V_L, J_{ij}^R > J_{b_1 b_2}^R\}; \\ G_R &:= (V_R, E_R), \quad \text{with } E_R := \{e_{ij} \in E; \mathbf{y}_i, \mathbf{y}_j \in V_R, J_{ij}^R > J_{b_1 b_2}^R\}. \end{aligned}$$

Then we find the dominant transition path in G_L from A to b_1 and in G_R from b_2 to B . So the computation of the dominant transition path is simply finding the bottleneck recursively.

In summary, we will first compute the committor function q by solving the linear system (4.14). Then we construct the graph $G(V, E)$, and compute the dominant transition path based on recursively finding the bottlenecks via Algorithm 2 and the dominant transition paths via Algorithm 3, see below for the details of the algorithmic constructions.

Algorithm 2: Algorithm for finding the bottleneck

Algorithm Inputs: Graph $G(V, E)$, starting and ending states $A, B \subset \mathcal{N}$.

- 1 Sort edges of G according to their weights in ascending order. We have $E_{\text{sort}} = \{e_1, e_2, \dots, e_{|E|}\}$.
 - 2 IF edge $e_{|E|}$ connects A and B , THEN RETURN bottleneck $b = e_{|E|}$.
 - 3 Initialize $l = 1$, $r = |E|$.
 - 4 WHILE $r - l > 1$:
 - 5 Set $m = (l + r)/2$, $E'(m) = \{e_m, e_{m+1}, \dots, e_{|E|}\}$.
 - 6 IF there exists a reaction pathway in $G(Q, E'(m))$.
 - 7 THEN $l = m$; ELSE $r = m$.
 - 8 ENDWHILE; RETURN $b = e_l$.
-

Algorithm 3: Algorithm for finding the most probable transition path

Algorithm Inputs: Graph $G(V, E)$, starting and ending states $A, B \subset \mathcal{N}$.

- 1 Given graph $G(V, E)$, A and B , determine bottleneck $b = (b_1, b_2)$.
- 2 Determine the disconnected subgraphs G_L and G_R as in (5.7).
- 3 Set

$$p_L = \begin{cases} b_1, & \text{if } b_1 \in A \\ \text{result of the recursion with } (G_L(V_L, E_L), A, \{b_1\}), & \text{if } b_1 \notin A. \end{cases}$$

and

$$p_R = \begin{cases} b_2, & \text{if } b_2 \in B \\ \text{result of the recursion with } (G_R(V_R, E_R), \{b_2\}, B), & \text{if } b_2 \notin B. \end{cases}$$

- 4 RETURN (p_L, p_R) .
-

5.3. Monte Carlo simulation based on the controlled random walk on point clouds.

Based on the effective potential U^e in (3.29) and the controlled Markov process with generator Q^q in (4.27), the transition between metastable states can be simulated more easily by the Monte Carlo simulations for the controlled random walk on point clouds. Under the dynamics governed by U^e , the exit from the attraction basin of metastable state A is almost sure. We will first generate a set of trajectories from A to B via Monte Carlo simulations for the controlled random walk, based on which, we then find the mean reactive path from A to B .

5.3.1. Generation of trajectories from A to B via the controlled random walk on point clouds.

We simulate a random walk $\{\mathbf{y}_t^q\}$ on point clouds based on the controlled generator Q^q in (4.27). In detail, we first extend the Markov process with $(Q^q)_{ij}$ in (4.27) to include the site i_a . Then we have $\lambda_{i_a}^q = +\infty$, so the waiting time at i_a is zero. Thus at $t = 0$, we start the simulation at $\mathbf{y}_0^q \in VF(i_a)$ with probability

$$(5.8) \quad P_{i_a j}^q = \frac{q_j(\pi_{i_a} + \pi_j)}{\mathcal{Z}} \frac{|\Gamma_{j i_a}|}{|y_{i_a} - y_j|}, \quad j \in VF(i_a), \quad \mathcal{Z} = \sum_{j \in VF(i_a)} q_j \frac{\pi_{i_a} + \pi_j}{|y_{i_a} - y_j|} |\Gamma_{i_a j}|.$$

In other words, $P_{i_a j}^q \propto J_{i_a j}^R$. We refer to [LN15, Lemma 1.3] for the reactive exit distribution on ∂A for the continuous Markov process. Suppose $\mathbf{y}_{t_k}^q = \mathbf{y}_i$, the next step is to update Δt_k and $\mathbf{y}_{t_{k+1}}^q$ as follows. (i) $\mathbf{y}_{t_k}^q$ jumps to $\mathbf{y}_j \in VF(\mathbf{y}_i)$ with probability $P_{ij}^q \equiv Q_{ij}^q / \lambda_i^q$, where λ_i^q is defined in (4.11); (ii) the waiting time $\Delta t_k = t_{k+1} - t_k \sim \mathcal{E}(\lambda_i^q)$ is an exponentially distributed random variable with rate λ_i^q . We repeat this simulation K times to obtain the data $\{\mathbf{y}_k^q, \Delta t_k\}_{k=0:K}$, in which we restart the simulation from A each time when we hit B . Denote a sampled trajectory part P_r of length r , from ∂A to B , as $P_r := \{(\mathbf{y}_0^q, \Delta t_0), (\mathbf{y}_1^q, \Delta t_1), \dots, (\mathbf{y}_r^q, \Delta t_r)\}$ such that $\mathbf{y}_0^q \in VF(i_a)$ and $\mathbf{y}_r^q \in B$. We summarize this simulation in Algorithm 4.

Algorithm 4: Algorithm for controlled random walk on point clouds

Algorithm Inputs: Maximum iteration K .

- 1 Set $k = 0, r = 0$. Generate $\mathbf{y}_0^q \in VF(i_a)$ with probability $P_{i_a j}$.
 - 2 $\mathbf{y}_{t_{k+1}}^q := \mathbf{y}_{t_k}^q = \mathbf{y}_s$, where $s = \min\{s | \sum_{j=1, j \neq i}^s P_{ij}^q \geq \eta\}$, where $\eta \sim U[0, 1]$ is a uniformly distributed random variable.
 - 3 $t_{k+1} = t_k + \Delta t_k$, Δt_k being an exponentially distributed random variable with rate λ_i^q .
 - 4 $k \leftarrow k + 1, r \leftarrow r + 1$. Repeat until $\mathbf{y}_r^q \in B$. Record the trajectory $P_r = \{(\mathbf{y}_0^q, \Delta t_0), \dots, (\mathbf{y}_r^q, \Delta t_r)\}$.
 - 5 Reset $r = 0, \mathbf{y}_r^q \in VF(i_a)$ according to Step 1. Repeat the above iterations until k exceeds the maximum iteration number K .
-

5.3.2. *Post-process for finding the mean transition path from A to B .* To find the mean transition path via a sequence of data $\{(\mathbf{y}_k^q, \Delta t_k)\}_{k=0:K}$ obtained from Algorithm 4, we design a local average mean path algorithm to move an initial connecting string from ∂A to B to the final converged mean transition path as follows. This mean path algorithm is particularly useful for the case that there are multiple transition paths.

For some M , we first initialize a discrete path $P^0 = \{p_m^0\}_{m=1:M}$ on manifold connecting A and B . For l -th iteration step and for any p_m^l , we select segments of reactive trajectories inside the ball $\mathcal{B}_{r_0}^{\mathbb{R}^\ell}(p_m^l)$, where the radius $r_0 > 0$ is chosen such that $\{\mathbf{y}_k^q\} \cap \mathcal{B}_{r_0}^{\mathbb{R}^\ell}(p_m^l)$ has enough samples. Denote the resulting samples as

$$(5.9) \quad \{\mathbf{y}_k^q\}_{k=0:M} \cap \mathcal{B}_{r_0}^{\mathbb{R}^\ell}(p_m^l) = \{\mathbf{y}_{r_1}^q, \dots, \mathbf{y}_{r_m}^q\}, \quad r_1, r_2, \dots, r_m \in \{0, 1, \dots, K\}.$$

Then we apply the ergodic theorem conditioned in the ball $\mathcal{B}_{r_0}^{\mathbb{R}^\ell}(p_m^l)$ to find out the observed spatial average \tilde{p}_m^{l+1} inside the ball $\mathcal{B}_{r_0}^{\mathbb{R}^\ell}(p_m^l)$. This is computed by the time average of those selected samples, associated with their waiting time, inside the ball

$$(5.10) \quad \tilde{p}_m^{l+1} := \frac{1}{\Delta T_l} \sum_{j=1}^m \mathbf{y}_{r_j}^q \Delta t_{r_j}, \quad \Delta T_l = \sum_{j=1}^m \Delta t_{r_j}.$$

Furthermore, in order to avoid the problem that all M discrete points overlap and concentrate on a few ones, an arc-length reparameterizing procedure similar to [ERVE02] is needed.

To do the reparameterization, we first compute

$$(5.11) \quad S_1 = 0, \quad S_m = \sum_{j=2}^m |\tilde{p}_m^{l+1} - \tilde{p}_{m-1}^{l+1}|, \quad m = 2, \dots, M.$$

Then the total length of \tilde{P}^{l+1} is approximately S_M . We do the arc-length reparameterizations by linear interpolation as follows. (i) Denote $L_m := \frac{m-1}{M-1}S_M$, $m = 1, 2, \dots, M$; (ii) find the index m' such that $S_{m'} \leq L_m < S_{m'+1}$; (iii) calculate the linear interpolation

$$(5.12) \quad p_m^{l+1} \approx \frac{L_m - S_{m'}}{S_{m'+1} - S_{m'}} \tilde{p}_{m'}^{l+1} + \frac{S_{m'+1} - L_m}{S_{m'+1} - S_{m'}} \tilde{p}_{m'+1}^{l+1}.$$

Here \approx means finding the nearest point on the manifold. Then we can obtain the new path $P^{l+1} = \{p_m^{l+1}\}_{m=1:M}$. This updating process can be iteratively repeated until converge, i.e., $P^{l+1} = P^l$ up to some tolerance. We summarize the above algorithm for finding mean transition path in Algorithm 5.

Algorithm 5: Finding mean transition path from A to B using simulation data.

Algorithm Inputs: Simulation data $\{\mathbf{y}_k^q\}_{k=0:K}$, waiting time $\{\Delta t_k\}_{k=0:K}$, radius $r_0 > 0$.

- 1 Set $l = 0$ and for some M , initialize a discrete path $P^l = \{p_m^l\}_{m=1:M}$ on manifold \mathcal{N} connecting A and B , where $p_m^l \in \mathcal{N}$.
 - 2 For every $1 \leq m \leq M$, collect all sample points in $\mathcal{B}_{r_0}^{\mathbb{R}^\ell}(p_m^l)$ based on (5.9).
 - 3 Update path \tilde{P}^{l+1} with the weighted average for $m = 1, \dots, M$ via (5.10).
 - 4 Compute S_1, \dots, S_M via (5.11).
 - 5 Update $P^{l+1} = \{p_m^{l+1}\}_{m=1:M}$ by arc-length reparameterization (5.12).
 - 6 $l \leftarrow l + 1$. Repeat until P^l converges or l exceeds a prescribed number L_{\max} .
-

5.4. Numerical results. We choose the Mueller potential on \mathbb{R}^2 as the illustrative example and map it to different manifolds. The Mueller potential on \mathbb{R}^2 is

$$(5.13) \quad U(X, Y) := \sum_{i=1}^4 A_i \exp(a_i(X - \alpha_i)^2 + b_i(X - \alpha_i)(Y - \beta_i) + c_i(Y - \beta_i)^2).$$

The parameters are set to be $A_{1-4} = -2, -1, -1.7, 0.15$, $a_{1-4} = -1, -1, -6.5, 0.7$, $b_{1-4} = 0, 0, 11, 0.6$, $c_{1-4} = -10, -10, -6.5, 0.7$, $\alpha_{1-4} = 1, 0, -0.5, -1$, $\beta_{1-4} = 0, 0.5, 1.5, 1$. Denote $\mathbf{X} = (X, Y)$. This potential has three local minima $\mathbf{X}_1, \mathbf{X}_2, \mathbf{X}_3$ and two saddle points $\mathbf{X}_4, \mathbf{X}_5$. The contour plot of the Mueller potential and the stationary points are shown in Fig. 1.

We are interested in the transitions from the metastable state \mathbf{X}_1 to \mathbf{X}_3 . Finding the transition path from \mathbf{X}_1 to \mathbf{X}_3 is a well-studied problem. One can compute the transition path by some existing methods like string method [ERVE02], etc., which is shown in Fig. 1.

Example 1: Mueller potential on sphere. We map the Mueller potential to $\mathcal{N} = \mathbb{S}^2$ by the stereographic projection $X = x/(1 - z)$, $Y = y/(1 - z)$. For any point $(x, y, z) \in \mathbb{S}^2$ except the north pole, we define $U_{\mathcal{N}}(x, y, z)$ on \mathbb{S}^2 as

$$U_{\mathcal{N}}(x, y, z) = U^S(x, y, z) = U\left(\frac{x}{1-z}, \frac{y}{1-z}\right), \quad (x, y, z) \in \mathbb{S}^2$$

and consider the transitions between two metastable states under the dynamics (1.1). It is easy to obtain that the invariant distribution of \mathbf{y}_t is $\pi(\mathbf{y}) \propto \exp(-\varepsilon^{-1}U^S(\mathbf{y}))$, $\mathbf{y} = (x, y, z)$. We then generate the data set $D = \{\mathbf{y}_i\}_{i=1:4000}$ uniformly on \mathbb{S}^2 and set $\pi_i = \exp(-\varepsilon^{-1}U^S(\mathbf{y}_i))$, respectively. We choose the starting state $A = D \cap \mathcal{B}_{0.05}^{\mathbb{R}^3}(\mathbf{X}_1)$ and the ending state $B = D \cap \mathcal{B}_{0.05}^{\mathbb{R}^3}(\mathbf{X}_3)$, where $\mathcal{B}_r^{\mathbb{R}^3}(\mathbf{x}) = \{\mathbf{y} \in \mathbb{R}^3 \mid \|\mathbf{y} - \mathbf{x}\| < r\}$ is the ball centered at \mathbf{x} with radius r in \mathbb{R}^3 . With this data set, we can compute the committor function $q(\mathbf{y})$ by solving the

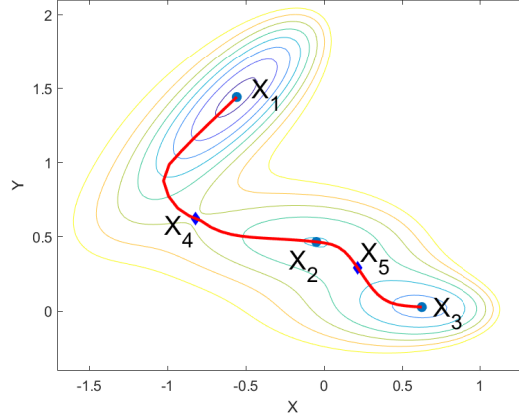


FIGURE 1. Contour plot of 2D Mueller potential $U(X, Y)$ in (5.13) and transition path from \mathbf{X}_1 to \mathbf{X}_3 . The blue dots are local minima $\mathbf{X}_{1,2,3}$. The blue diamonds are saddle points $\mathbf{X}_{4,5}$. The red line is the transition path obtained by string method.

approximated Voronoi tessellation via Algorithm 1 and the linear system (4.14). Since it is a diagonally dominant system, the solution is unique and we utilize a diagonal preconditioning trick to make the computation more effective and stable.

The effective potential U^e with $\varepsilon = 0.1$ is shown in Fig. 2. Under the controlled random walk (4.25), the transition from A to B happens much easier. One can see from the Monte Carlo simulation in Fig. 2 (c), the exit from the attraction basin of metastable state \mathbf{X}_1 is almost sure rather than a rare event. Compared with the original $U^S(\mathbf{y})$, in the effective potential, the local minima at A disappears and U^e tends to infinity when approaching A ; see Fig. 2(b). We can also find that the dominant transition path almost goes along the gradient direction of U^e from A to B . Taking the maximum iteration $K = 10^5$ in the Monte Carlo simulation Algorithm 4, we find 48 transition trajectories from A to B ; see Fig. 2(c). In the simulation with the uncontrolled generator Q , there is no transition from A to B at all in 10^5 steps. The mean transition path based on Algorithm 5 is also shown using the solid black line in Fig. 2(c). We set $M = 100$ and $L_{\max} = 20$ in the algorithm. The mean transition path derived by Monte Carlo simulation data (the solid black line in Fig. 2(c)) highly coincides with the dominant transition path in TPT (red circles in Fig. 2(c)).

With committor function $q(\mathbf{y})$, we can obtain the dominant transition path by applying Algorithms 2-3. We show the results for different ε in Fig. 3(a)-(c). As a comparison, we also compute the minimum energy path in the limit $\varepsilon \rightarrow 0$. This can be done by minimizing the Freidlin-Wentzell action functional [FW12]. Namely, it is the solution of the following variational problem

$$(5.14) \quad S(B; A) = \inf_{T > 0} \inf_{\mathbf{x} \in A, \mathbf{y} \in B} \inf_{\psi(t) \subset \mathcal{N}: \psi(0) = \mathbf{x}, \psi(T) = \mathbf{y}} \int_0^T \left\| \dot{\psi} + \nabla_{\mathcal{N}} U(\psi) \right\|^2 dt.$$

This problem can be efficiently solved by minimum action method (MAM) on manifold [ERVE04, LLZ16]. Note that $U^S(x, y, z)$ can be naturally extended to $\mathbb{R}^3 \setminus \{z = 1\}$, one can directly apply MAM on \mathcal{N} by a properly designed MAM on \mathbb{R}^3 . This zero-noise path is used as a reference; see solid red line in Fig. 3. We also map the transition path on \mathcal{N} to \mathbb{R}^2 by the stereographic projection. The result is shown in Fig. 3(d)-(f).

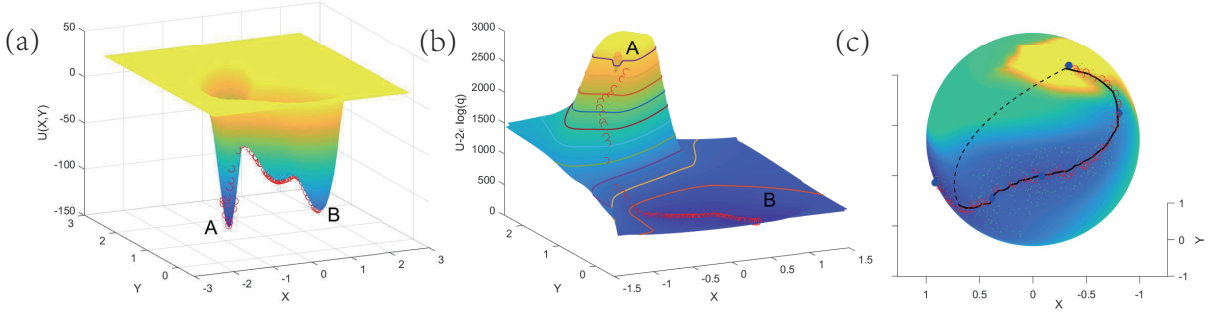


FIGURE 2. Projections of the Mueller potential and the effective potential on \mathbb{S}^2 to \mathbb{R}^2 . (a) the projection of $U^S(x, y, z)$ to \mathbb{R}^2 . (b) the projection of effective potential $U^e = U^S - 2\varepsilon \log q$ to \mathbb{R}^2 . The contour lines of U^e are shown in colored lines. The hole at A is due to $U^e(A) = +\infty$. (c) The Monte Carlo simulation result of transition from A to B based on effective backward operator Q^q and the mean transition path. The background is heat plot of U^e . The green dots are Monte Carlo samples. The black line is the mean transition path computed by Algorithm 5 while the dashed line is the initial discrete path. In all sub-figures, the dominant transition paths are shown with red circles.

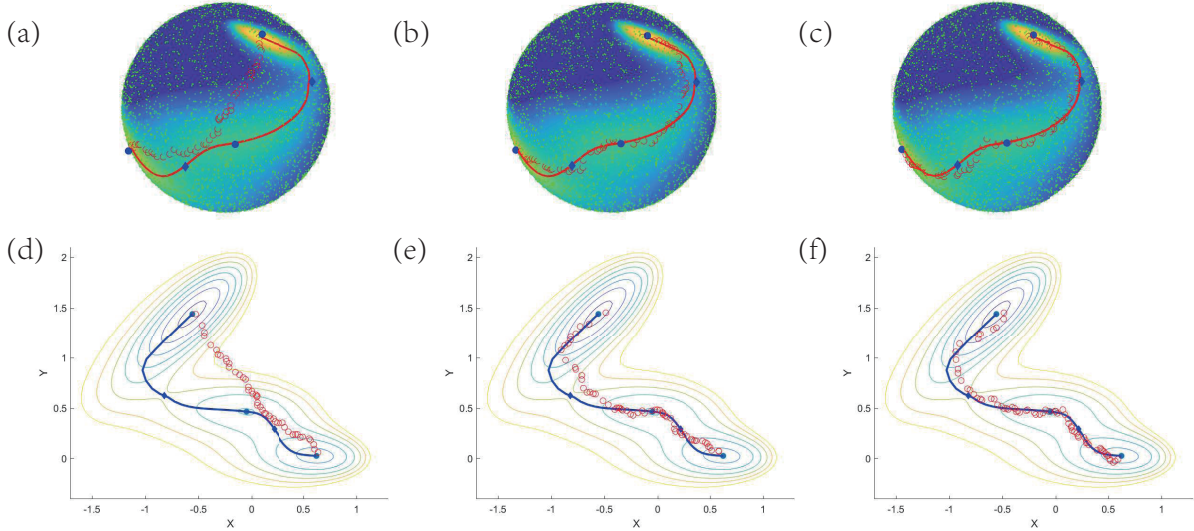


FIGURE 3. The dominant transition paths from \mathbf{X}_1 to \mathbf{X}_3 on \mathbb{S}^2 for different ε . (a)(d) $\varepsilon = 1$. (b)(e) $\varepsilon = 0.2$. (c)(f) $\varepsilon = 0.05$. In all sub-figures, the blue dots are metastable states $\mathbf{X}_{1,2,3}$ while the blue diamonds are saddle points. (a)-(c) The background of each sub-figure shows the heat plot of $U^S(x, y, z)$. The small green dots are 4000 random samples. The paths of red circles are dominant transition paths obtained by TPT. The zero-noise minimum energy paths computed by MAM are shown with solid red lines. (d)-(f) The background is the contour plot of potential $U(X, Y)$. The solid blue lines and red circles are the projections of transition paths in (a)-(c), respectively.

In Fig. 3, we find that as ε tends to zero, the dominant transition path converges to the zero-noise path obtained by MAM both on manifold \mathbb{S}^2 and the 2D projection. This is consistent with the Freidlin-Wentzell theory. The results are stable when different random samples are utilized.

We can find some critical transition states along the dominant transition path with the help of probability current J^R . Note that finding the dominant transition path is a divide-and-conquer algorithm by finding a sequence of dynamical bottlenecks via Algorithm 3. The key transition states must have the least current J^R . In Fig. 4, we plot the current J^R along the dominant transition path. The states with the least five J^R are marked and projected to \mathbb{R}^2 , ε is chosen to be 0.1. One can see that all these five states are in neighbourhoods of saddle points or local minima. As stated by the Freidlin-Wentzell theory, the transition path in the zero noise limit must pass through stationary points, which is confirmed in our computations.

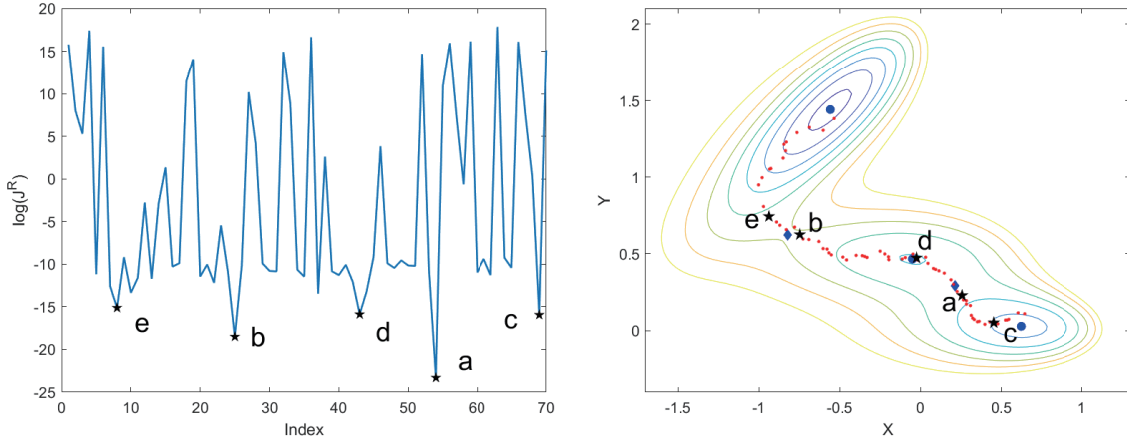


FIGURE 4. The key transition states along dominant transition path, $\varepsilon = 0.1$. Left panel: the $\log J^R$ along dominant transition path. The states with the least five J^R are marked by a-e in ascending order. Right panel: the projection of dominant transition path on \mathbb{R}^2 . This sub-figure is similar as (d)-(f) of Fig. 3 except that the dominant transition path is marked with red dots. The five states in the left panel are also marked in this sub-figure.

The transition rate calculated by (4.18) is also consistent with the Freidlin-Wentzell theory. When A, B are metastable states, it is well known that as $\varepsilon \rightarrow 0$, $\varepsilon \log k_{AB} \rightarrow S(B; A)$, where $S(B; A)$ in (5.14) is the so-called quasi-potential. The value of $S(B; A)$ is a side product when computing the minimum energy path on manifold \mathcal{N} by MAM. The rescaled rates k_{AB} for different ε and $S(B; A)$ are listed in Table 1. We can find that as ε becomes smaller, the transition rates calculated by (4.18) get closer to the quasi-potential.

	$\varepsilon = 1$	$\varepsilon = 0.2$	$\varepsilon = 0.05$	$\varepsilon = 0.02$	$S(B; A)$
$\varepsilon \log k_{AB}$	-0.4282	0.2540	0.3979	0.3999	0.3816

TABLE 1. Comparison of the transition rates obtained by TPT and the quasi-potential.

Example 2: Mueller potential on torus. We can also map the Mueller potential to the torus $\mathcal{N} = \mathbb{T}^2$ which is defined as

$$x = (R + r \cos \theta) \cos \phi, \quad y = (R + r \cos \theta) \sin \phi, \quad z = r \sin \theta, \quad \theta \in [-\pi, \pi), \phi \in [0, 2\pi).$$

Set $R = 2.0, r = 1.0$. We define the potential $U_{\mathcal{N}}$ on torus as

$$U_{\mathcal{N}}(x, y, z) = U^{\text{tor}}(x, y, z) := U(r\theta, R\phi).$$

We also consider the transitions from $A = D \cap \mathcal{B}_{0.05}^{\mathbb{R}^3}(\mathbf{X}_1)$ to $B = D \cap \mathcal{B}_{0.05}^{\mathbb{R}^3}(\mathbf{X}_3)$. The data set $D = \{\mathbf{y}_i\}_{i=1:4000}$ is generated uniformly on \mathbb{T}^2 and $\pi_i = \exp(-\varepsilon^{-1}U^{\text{tor}}(\mathbf{y}_i))$. The referenced zero-noise minimum energy path can also be calculated by MAM on the manifold with the natural extension of $U^{\text{tor}}(\mathbf{y})$ to $\mathbb{R}^2/\mathbb{Z}^2$. By applying Algorithms 1-3, the dominant transition paths for different ε are shown in Fig. 5 using red circles. Similar as in the sphere case, we observe that the dominant transition paths converge to the zero-noise path as ε tends to 0.

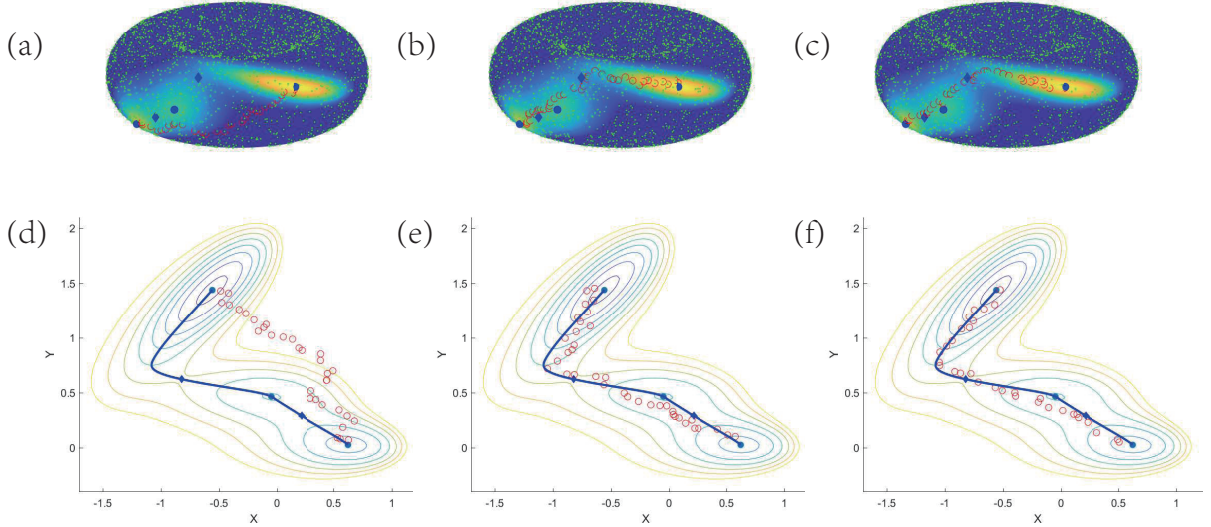


FIGURE 5. The dominant transition paths from \mathbf{X}_1 to \mathbf{X}_3 on torus \mathbb{T}^2 for different ε . (a)(d) $\varepsilon = 1$. (b)(e) $\varepsilon = 0.2$. (c)(f) $\varepsilon = 0.05$. All of the utilized symbols and paths are similar to Fig. 3 except that the considered potentials are $U^{\text{tor}}(x, y, z)$ on \mathbb{T}^2 .

It is interesting to study the transition behavior of dynamics (1.1) with finite but small noise and the driving potential are also perturbed by noise with similar scales. In this case, minimizing the Freidlin-Wentzell action functional is not proper because the effect of finite noise is ignored. Finite temperature string method [ERVE05] is a good candidate for this problem. However, it is not straightforward to apply this method on a manifold.

Instead, we can still study this problem by TPT on point clouds. We perturb the Mueller potential by small oscillations as

$$\tilde{U}(X, Y) = U(X, Y) + 0.15 \sin(10\pi X) \sin(10\pi Y)$$

and define the perturbed potential $U_{\mathcal{N}}$ on torus by

$$U_{\mathcal{N}}(x, y, z) = \tilde{U}^{\text{tor}}(x, y, z) := \tilde{U}(r\theta, R\phi).$$

We choose $\varepsilon = 0.1$, which is in the same scale of our perturbations. By using 4000 uniform random samples on \mathbb{T}^2 , we obtain the dominant transition paths as shown with red circles in Fig. 6. For a reference, we still plot the minimum energy path under zero noise and zero perturbation in (b).

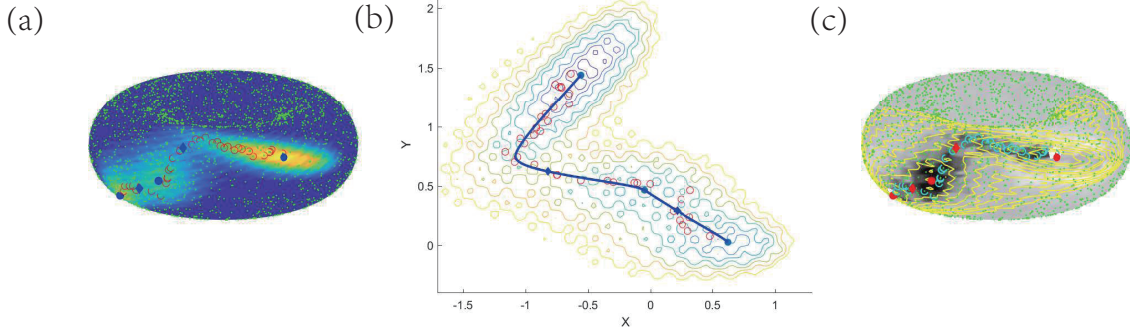


FIGURE 6. The dominant transition path from \mathbf{X}_1 to \mathbf{X}_3 on torus under perturbed Mueller potential ($\varepsilon = 0.1$). In three sub-figures, The metastable states and saddle points are shown with blue dots and diamonds, respectively. (a) The background shows the heat plot of $\tilde{U}^{\text{tor}}(x, y, z)$. (c) The background shows the density of transition paths ρ_R in log scale. The yellow lines correspond to the contour of $\tilde{U}^{\text{tor}}(x, y, z)$. In both sub-figures, the small green dots are 4000 random samples, and the path of red/cyan circles is the dominant transition path. (b) The background is the contour plot of the perturbed Mueller potential $\tilde{U}(X, Y)$. The red circles and blue solid line correspond to the projection of dominate transition path and the reference zero-noise minimum energy path, respectively.

Compared with Fig. 5, although the potential is perturbed, TPT can still find the dominant transition behavior similar as the non-perturbed case. The noise effect on the potential is eliminated and we can still capture the main transition behavior from \mathbf{X}_1 to \mathbf{X}_3 . We can find from Fig. 6(c) that although the landscape is rough, the density of transition path ρ_R is relatively smooth. The dominant transition path lies in the domain with largest value of ρ_R .

6. CONCLUSION

We reinterpreted the transition state theory and the transition path theory from the optimal control viewpoint and designed a data-driven solver for finding transition paths on manifolds. The optimal controlled random walk on point clouds realizes the original rare events almost surely, which enables the efficient computations for the mean transition path based on the Monte Carlo simulations.

ACKNOWLEDGEMENTS

The authors would like to thank Prof. Weinan E for valuable suggestions. J.-G. Liu was supported in part by NSF under award DMS-1812573. T. Li was supported by the NSFC under grants Nos. 11421101 and 11825102, and Beijing Academy of Artificial Intelligence (BAAI). X. Li was supported by the construct program of the key discipline in Hunan Province.

REFERENCES

- [CL06] Ronald R Coifman and Stéphane Lafon. Diffusion maps. *Applied and computational harmonic analysis*, 21(1):5–30, 2006.
- [DS01] Jean-Dominique Deuschel and Daniel W Stroock. *Large deviations*. American Mathematical Society, Rhode Island, 2001.
- [ERVE02] Weinan E, Weiqing Ren, and Eric Vanden-Eijnden. String method for the study of rare events. *Phys. Rev. B*, 66(5):052301, 2002.
- [ERVE04] Weinan E, Weiqing Ren, and Eric Vanden-Eijnden. Minimum action method for the study of rare events. *Comm. Pure Appl. Math.*, 57(5):637–656, 2004.
- [ERVE05] Weinan E, Weiqing Ren, and Eric Vanden-Eijnden. Finite temperature string method for the study of rare events. *J. Phys. Chem. B*, 109(14):6688–6693, 2005.
- [Eva10] Lawrence C Evans. *Partial differential equations*, volume 19. American Mathematical Society, Rhode Island, 2010.
- [Eva13] Lawrence C Evans. *An Introduction to Stochastic Differential Equations*. American Mathematical Society, Rhode Island, 2013.
- [EVE06] Weinan E and Eric Vanden-Eijnden. Towards a theory of transition paths. *J. Stat. Phys.*, 123(3):503, 2006.
- [EVE10] Weinan E and Eric Vanden-Eijnden. Transition-path theory and path-finding algorithms for the study of rare events. *Ann. Rev. Phys. Chem.*, 61(1):391–420, Mar 2010.
- [FS06] Wendell H Fleming and Halil Mete Soner. *Controlled Markov processes and viscosity solutions*. Springer Science & Business Media, New York, 2nd edition, 2006.
- [FW12] Mark I. Freidlin and Alexander D. Wentzell. *Random Perturbations of Dynamical Systems*, volume 260 of *Grundlehren der mathematischen Wissenschaften*. Springer Berlin Heidelberg, 2012.
- [GLW20] Yuan Gao, Jian-Guo Liu, and Nan Wu. Data-driven efficient solvers and predictions of conformational transitions for langevin dynamics on manifold in high dimensions. *arXiv preprint arXiv:2005.12787*, 2020.
- [HBS⁺13] Carsten Hartmann, Ralf Banisch, Marco Sarich, Tomasz Badowski, and Christof Schütte. Characterization of rare events in molecular dynamics. *Entropy*, 16(1):350–376, Dec 2013.
- [HRSZ17] Carsten Hartmann, Lorenz Richter, Christof Schütte, and Wei Zhang. Variational characterization of free energy: Theory and algorithms. *Entropy*, 19(11):626, Nov 2017.
- [HS12] Carsten Hartmann and Christof Schütte. Efficient rare event simulation by optimal nonequilibrium forcing. *J. Stat. Mech.: Theory Exp.*, 2012(11):P11004, Nov 2012. arXiv: 1208.3232.
- [HSZ16] Carsten Hartmann, Christof Schütte, and Wei Zhang. Model reduction algorithms for optimal control and importance sampling of diffusions. *Nonlinearity*, 29(8):2298–2326, Aug 2016.
- [LL18] Rongjie Lai and Jianfeng Lu. Point cloud discretization of fokker-planck operators for committor functions. *Multiscale Modeling & Simulation*, 16(2):710–726, Jan 2018.
- [LLL19] Anning Liu, Jian-Guo Liu, and Yulong Lu. On the rate of convergence of empirical measure in ∞ -wasserstein distance for unbounded density function. *Quart. Appl. Math.*, 77(4):811–829, 2019.
- [LLZ16] Tiejun Li, Xiaoguang Li, and Xiang Zhou. Finding transition pathways on manifolds. *Multiscale Model. Simul.*, 14(1):173–206, Jan 2016.
- [LN15] Jianfeng Lu and James Nolen. Reactive trajectories and the transition path process. *Probab. Theory Relat. Fields*, 161(1–2):195–244, Feb 2015.
- [MSVE06] Philipp Metzner, Christof Schütte, and Eric Vanden-Eijnden. Illustration of transition path theory on a collection of simple examples. *J. Chem. Phys.*, 125(8):084110, Aug 2006.
- [MSVE09] Philipp Metzner, Christof Schütte, and Eric Vanden-Eijnden. Transition path theory for markov jump processes. *Multiscale Model. Simul.*, 7(3):1192–1219, Jan 2009.
- [TS15] Nicolás García Trillos and Dejan Slepčev. On the rate of convergence of empirical measures in ∞ -transportation distance. *Canadian J. Math.*, 67(6):1358–1383, 2015.
- [Var07] Sathamangalam R Srinivasa Varadhan. *Stochastic Processes*. American Mathematical Society, Rhode Island, 2007.

DEPARTMENT OF MATHEMATICS, DUKE UNIVERSITY, DURHAM, NC

Email address: `yuangao@math.duke.edu`

LMAM AND SCHOOL OF MATHEMATICAL SCIENCES, PEKING UNIVERSITY, BEIJING 100871, CHINA

Email address: `tieli@pku.edu.cn`

MOE-LCSM, SCHOOL OF MATHEMATICS AND STATISTICS, HUNAN NORMAL UNIVERSITY, CHANGSHA 410081,
CHINA

Email address: `lixiaoguang@hunnu.edu.cn`

DEPARTMENT OF MATHEMATICS AND DEPARTMENT OF PHYSICS, DUKE UNIVERSITY, DURHAM, NC

Email address: `jliu@math.duke.edu`